

Development of Novel Ex Vivo Assays to Characterize the Mechanical Properties of Blood
Plasma Clots

A Thesis

Presented to
the faculty of the School of Engineering and Applied Science
University of Virginia

in partial fulfillment
of the requirements for the degree

Master of Science

by

Matthew Joseph Perez

May

2015

APPROVAL SHEET

The thesis
is submitted in partial fulfillment of the requirements
for the degree of
Master of Science


AUTHOR

The thesis has been read and approved by the examining committee:

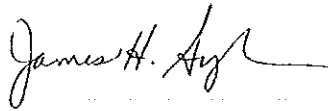
Michael Lawrence, PhD

Advisor

Brian Helmke, PhD

David Green, PhD

Accepted for the School of Engineering and Applied Science:



Dean, School of Engineering and Applied Science

May
2015

Development of Novel *Ex Vivo* Assays to Characterize the Mechanical Properties of Blood Plasma Clots

Blood coagulation is a life preserving process that operates in a narrow regime between thrombosis and hemorrhage. Inappropriate and inadequate blood clotting can lead to heart attack, stroke, and surgical bleeding, all potentially fatal conditions. Due to the large negative impact of inappropriate blood clotting, it is necessary to characterize normal plasma clot structure and properties to better understand abnormal conditions as well as develop strategies to control bleeding and prevent thrombosis.

Activation of the coagulation cascade transforms blood from a viscous liquid to a porous viscoelastic gel of crosslinked fibrin fibers and platelets. The ability, or inability, of a blood clot to perform its necessary function is linked to the mechanical properties of the fibrin/platelet network. This work describes two novel *ex vivo* assays to characterize the mechanical properties of blood plasma clots; a passive microrheology assay and an optical microscopy – ultrasound acoustic radiation force (ARF) coupled assay are detailed here.

The passive microrheology assay utilizes single particle tracking of microspheres dispersed within a small volume plasma sample (approximately 15 μL) to calculate the mean squared displacement (MSD) of the particle. MSD can be used to calculate the diffusivity of the particle and the viscoelastic modulus of the plasma sample. The passive microrheology assay can also be coupled with fluorescence microscopy of the fibrin network to establish structure-function relationships.

The ARF-based assay is a non-contact method of strain application in blood plasma clots. Acoustically reflective microspheres dispersed in the sample act as force transducers and strain gauges. Ultrasound ARF is used to induce microsphere

displacement within a plasma sample and the displacement, coupled with a known magnitude of ARF application, is used to calculate clot stiffness. The assays described in this work can be used to characterize blood plasma clots under normal as well as perturbed conditions and demonstrate discernible differences in clot mechanical properties when platelet and fibrin polymerization inhibitors are used.

Acknowledgements

I would like to thank my advisor, Dr. Michael Lawrence, for his continued support and guidance throughout the completion of this project. His input and knowledge have been invaluable. I would also like to thank Dr. Brian Helmke, Dr. David Green, Dr. Francesco Viola, and Dr. Elisa Ferrante for their continuous feedback, advice, and mentoring.

I would also like to thank my labmates and friends in the department for their contributions to my work and their friendship. Finally, I want to thank my family for their continuous love and support throughout my education.

Table of Contents

Abstract	i
Acknowledgements	iii
Table of Contents	iv
List of Figures and Tables	v
Chapter 1. Introduction	1
1.1 Blood Coagulation and Thrombus Development	1
1.1.1 Normal Fibrin Polymerization and Binding to Platelets.....	2
1.1.2 Coagulation Inhibitors	3
1.2 Current Blood Coagulation Assessment Techniques	5
1.3 Novel Assay Development	6
Chapter 2. Passive Microrheology Assay..	9
2.1 Background	9
2.1.1 Brownian Thermal Motion and Mean Squared Displacement	9
2.1.2 Dynamic Modulus	12
2.2 Methods	13
2.2.1 Experimental Setup	13
2.2.2 Data Analysis	14
2.3 Results	15
2.3.1 Mean Squared Displacement and Effective Diffusivity.	15
2.3.2 Fluorescence Images	23
2.4 Discussion	29
Chapter 3. Acoustic Radiation Force Assay	32
3.1 Background	32
3.2 Methods	33
3.2.1 Experimental Setup	33
3.2.2 Data Analysis	37
3.3 Results	38
3.3.1 Microsphere Displacement	38
3.3.2 Clot Stiffness	40
3.4 Discussion	42
References	44

List of Figures and Tables

Figure 1.1:	Blood coagulation cascade diagram	2
Figure 1.2:	Normal platelet activation.....	3
Figure 1.3:	GPRP inhibition of fibrin polymerization.....	4
Figure 2.1:	Brownian thermal motion of a particle	10
Figure 2.2:	Sample preparation and experimental setup.....	14
Figure 2.3:	MSD of microspheres in PRP	17
Figure 2.4:	MSD of microspheres in 2mM GPRP	18
Figure 2.5:	MSD of microspheres in 4mM GPRP	19
Figure 2.6:	MSD of microspheres in ReoPro.....	20
Figure 2.7:	Power law curve fit to MSD data	21
Figure 2.8:	Effective diffusivity of microspheres in plasma	22
Figure 2.9:	Effective diffusivity of microspheres in plasma	23
Figure 2.10:	Fluorescence image of an untreated PRP clot	24
Figure 2.11:	Fluorescence image of a GPRP (2mM) treated plasma clot	25
Figure 2.12:	Fluorescence image of a GPRP (4mM) treated plasma clot	25
Figure 2.13:	Structural analysis of an untreated PRP clot	27
Figure 2.14:	Structural analysis of an a ReoPro (18 μ g/mL) treated clot	28
Figure 3.1:	Custom sample holder used in the ARF based assay	34
Figure 3.2:	ARF based assay experimental setup	35
Figure 3.3:	Force estimation of ARF magnitude using viscosity standards	38
Figure 3.4:	Characteristic microsphere displacement due to applied ARF	40
Figure 3.5:	Clot stiffness in untreated PRP and ReoPro treated PRP	41

Figure 3.6:	Comparison of clot stiffness in PRP and PPP	41
Table 2.1:	Quantification of fluorescence image analysis	29

Chapter 1: Introduction

1.1 Blood Coagulation and Thrombus Development

Blood coagulation is a life saving process that operates in a narrow regime between clot formation that obstructs blood vessels (thrombosis) and uncontrolled bleeding (hemorrhage) (1). Activation of the coagulation cascade (2) transforms blood from a viscous liquid to a porous viscoelastic gel of crosslinked fibrin fibers as seen in Figure 1.1. Effective blood clot formation requires an increase in material stiffness, a characteristic that can be correlated with clinical coagulopathies (3, 4).

Insufficient clot stiffness, or a 'soft' clot, is seen in hemorrhagic disorders such as hemophilia and is often observed clinically as surgical bleeding after invasive procedures such as cardiopulmonary bypass (5, 6). 'Hard' clots, in contrast, have been linked to the formation of thrombi in stroke, myocardial infarction, embolism, and deep vein thrombosis (1, 7-10).

Due to the large negative impacts of inappropriate blood clotting, it is necessary to characterize the contributions of platelets and the fibrin fiber network to normal and abnormal blood clot mechanical properties to better understand the coagulation process as well as develop strategies to control bleeding and prevent thrombosis. In order to characterize platelet and fibrin contributions to clot stiffness measurement techniques and assays must be developed that are sensitive enough to detect platelet and fibrin perturbations.

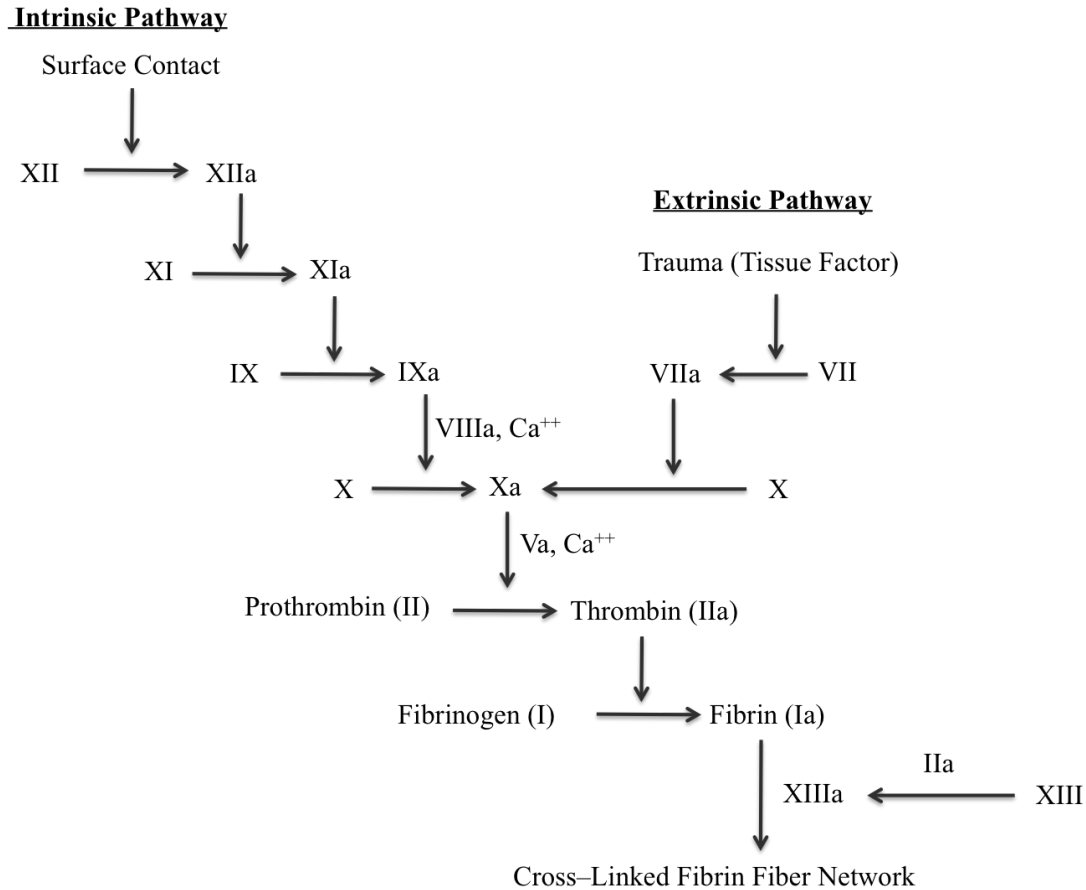


Figure 1.1: Blood coagulation cascade diagram. Coagulation is activated by one of two pathways, which convert soluble clotting proteins dissolved in blood plasma, known as clotting factors, to their active forms. The cascade ultimately yields a cross-linked fibrin fiber clot.

1.1.1 Normal Fibrin Polymerization and Binding to Platelets

Fibrinogen consists of 6 polypeptide chains held together by 29 disulfide bonds (11). Fibrin polymerization is initiated by cleavage of fibrinopeptides from fibrinogen to produce a fibrin monomer. Fibrinopeptide cleavage exposes an N-terminal motif Gly-Pro-Arg (GPR), called a knob, which can bind to a hole located in another fibrin molecule. Fibrin monomers aggregate and polymerize into fibrin protofibrils and fibers by attachment of fibrin monomers to each other through, ‘knob-hole’ interactions (shown in Figure 1.3) (11, 12).

Integrin $\alpha_{IIb}\beta_3$ on the platelet membrane plays a vital role in the formation of a cross-linked fibrin fiber network by serving as the cell surface receptor for fibrinogen. Integrin $\alpha_{IIb}\beta_3$ is a heterodimeric cell surface receptor comprised of two glycoprotein subunits (13, 14). After exposure to a platelet activator such as thrombin, adenosine diphosphate, or damaged blood vessels, platelets become activated and integrin $\alpha_{IIb}\beta_3$ undergoes a conformational change allowing fibrinogen to bind to the receptor, as shown in Figure 1.2 (15). Fibrinogen binding to integrin $\alpha_{IIb}\beta_3$ is a key step in platelet aggregation as well as cross-linking of the fibrin fiber network.

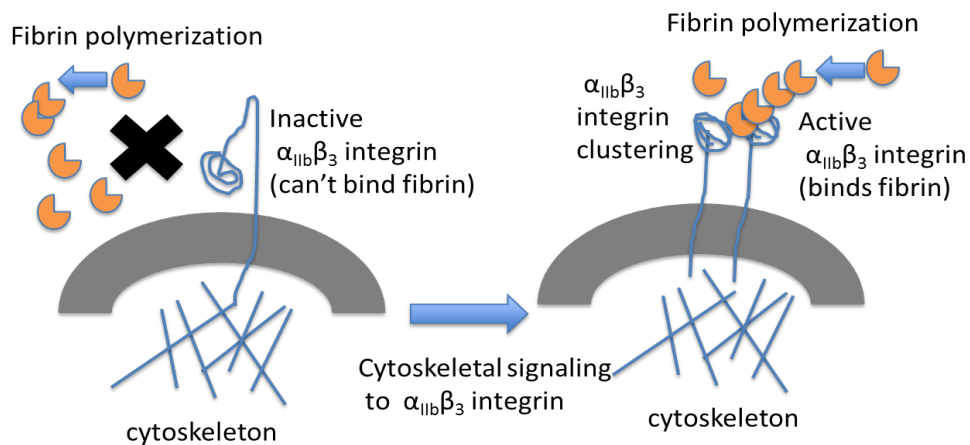


Figure 1.2: Normal platelet activation, integrin conformational change and fibrinogen binding to activated integrins, and fibrin fiber polymerization.

1.1.2 Coagulation Inhibitors

Coagulation inhibitors are molecules that inhibit or prevent the formation of a blood clot, depending on the inhibitor and the concentration in which it is used. Inhibitors target many aspects of the coagulation cascade including coagulation factors, fibrin fiber polymerization, thrombin formation, and platelets (16). In this work, two coagulation inhibitors were used, ReoPro (abciximab) and a Gly-Pro-Arg-Pro (GPRP) peptide.

ReoPro is a human-murine chimeric monoclonal antibody fab fragment that binds selectively to activated $\alpha_{IIb}\beta_3$ integrins on the platelet surface, preventing fibrinogen from binding to the integrin (17-19). ReoPro is a fairly large molecule, approximately 68 KDa, and effectively blocks fibrinogen from binding to the platelet through steric hinderance (17, 20, 21). The ReoPro binding site on $\alpha_{IIb}\beta_3$ is the RGD binding pocket and the secondary fibrinogen binding site (lysine-glutamine-alanine-glycine-aspartate-valine) (17). Because the binding of fibrinogen is an essential step in platelet aggregation, inhibition of $\alpha_{IIb}\beta_3$ with ReoPro directly inhibits the formation of a platelet aggregate, and may inhibit cross-linking of the fibrin fiber network.

GPRP is a tetrapeptide that mimics a fibrin monomer 'knob' (GPR motif) and binds to the 'holes' on a fibrin monomer, preventing the formation of fibrin protofibrils and fibrin fibers, as shown in Figure 1.3 (12, 22). The GPRP peptide is a competitive fibrin polymerization inhibitor, and can eliminate fibrin polymerization completely when used in high enough concentrations (approximately 8 mM) (23).

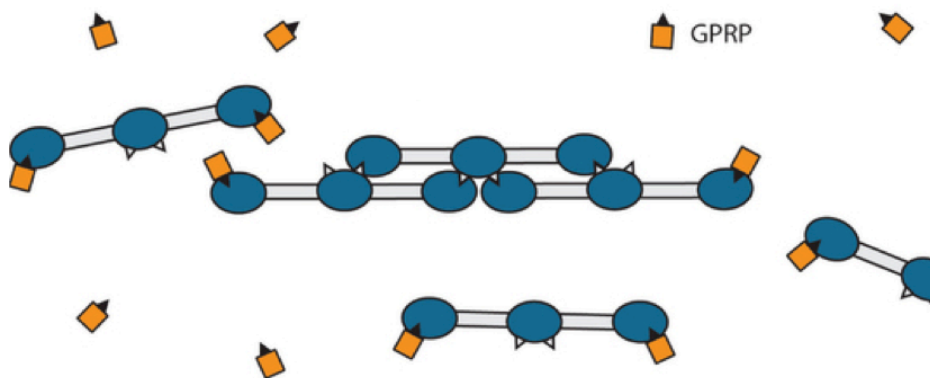


Figure 1.3: GPRP binding to 'holes' in the fibrin monomer, inhibiting the normal 'knob-hole' interaction between fibrinopeptides and their binding sites on fibrin monomers. Originally published by Chernysh et al. in Scientific Reports (2012).

1.2 Current Blood Coagulation Assessment Techniques

Several *ex vivo* methods to measure blood clot mechanical properties have successfully transitioned from the bench top into the clinic. Thromboelastography (TEG™) and rotational thromboelastometry (ROTEM™) are the two most prominent blood analysis technologies currently used in the clinic. Both TEG and ROTEM utilize oscillatory shear flow through rotational rheometry to assess coagulation in whole blood. Measurement of bulk clot stiffness by either the TEG or ROTEM can be used to assess the relative contributions of platelets and soluble coagulation factors to overall clot stiffness (24-26). However, neither TEG nor ROTEM measure clot stiffness directly and may introduce strain hardening in blood samples (27, 28).

Numerous other technologies are being developed from a variety of approaches to assess the mechanics of blood clotting both *in vivo* and *ex vivo*. Dynamic light scattering analysis has been used to measure *in vivo* blood coagulation by comparing motion of RBCs in flow or in stasis (29) and laser speckle rheology has been used to correlate changes in light scattering speckle intensity with viscoelastic property changes *ex vivo* (30). Recently, high resolution measurements of individual platelet contractility and fibrin fiber stiffness have given additional insight into the cellular and molecular basis of clot mechanics, though single cell and molecular assessments have yet to be linked to bulk rheological properties of clots (9, 31).

In contrast to approaches to assess *ex vivo* blood clot stiffness based on either light scattering or mechanical testing, ultrasound can assess tissue stiffness by generation of acoustic radiation force (ARF), which transfers momentum from the ultrasound waves to the propagating medium and any embedded reflective or absorptive objects (32-34). ARF

has been previously used to characterize the viscoelastic properties of various biological tissues including the liver, tumor tissue, and the vitreous body of the eye (34-37). In a more recent development to assess viscoelastic properties of blood, ultrasound ARF is coupled with echo time delay estimation of red blood cell displacement in a technique called sonorheometry (23, 38, 39).

1.3 Novel Assay Development

This work describes the development and validation of two novel assays to assess blood plasma coagulation. A passive microrheology assay and an optical microscopy - acoustic radiation force coupled assay are described, which aim to characterize the micro-scale and macro-scale mechanical properties of plasma clots, respectively. Both assays rely on optical detection of microsphere motion by video microscopy and thus require the use of plasma, opposed to whole blood. The high concentration of red blood cells in whole blood renders optical detection of microspheres impossible. So, RBCs are removed by centrifugation and blood plasma is characterized. This work aims to develop tools that can be used to elucidate the contributions of blood platelets and fibrin network properties, such as fiber diameter, porosity, tortuosity, and fiber density to the mechanical properties of blood plasma clots.

The passive microrheology assay is an *ex vivo* assay which provides a non-destructive method of testing the micro-scale mechanical properties a plasma clot during and after coagulation. The method utilizes the well-characterized theory of Brownian thermal motion and does not require application of external forces. Microscopic tracer particles are tracked using video microscopy and their motion is used to calculate their

mean squared displacement (MSD). The MSD can be used to calculate the diffusivity of the particle and can also be used to characterize the viscoelastic modulus of the material. That is, the MSD can be used to determine whether a material is purely viscous or viscoelastic in nature.

The application of passive microrheology in coagulating plasma is novel in that Brownian thermal motion has not been examined in blood plasma and has not been used to characterize changes in mechanical properties with time. Generally, passive microrheology is utilized to characterize polymeric solutions, viscous fluids, and colloidal solutions that are unchanging during the time scale of the measurement. This work demonstrates the utility of passive microrheology as a tool to assess materials with dynamic material properties. A novel measurement of effective diffusivity of microspheres in human plasma is also reported.

The passive microrheology assay can be combined with fluorescence imaging in a novel manner to observe the fibrin fiber network and obtain structural information about the plasma clot. When coupled with fluorescence imaging, the passive microrheology assay can be used to describe structure-function relationships between the elements of a plasma clot. Coagulation inhibitors can be added to the clotting plasma sample to observe the effects of the perturbation on clot mechanical properties as well as structural properties.

The ARF-based assay is a non-contact method of strain application to blood plasma clots that can be used to test their macro-scale mechanical properties. Acoustically reflective microspheres dispersed in blood plasma act as force transducers and strain gauges. Ultrasound ARF is used to induce microsphere displacement within a plasma

sample and the displacement is tracked by video microscopy to evaluate clot stiffness. A focused ultrasound transducer is used to perturb a small region of the sample such that it measures blood clot stiffness at an intermediate length scale between the milliliter volumes of conventional rheometric approaches and micro-scale approaches such as optical tweezers, atomic force microscopy (AFM), and passive microrheology. ARF-based assessment of clot stiffness is therefore useful for investigating the cooperative role of platelet signaling and fibrin dynamics in the viscoelastic transformation of a blood clot.

Chapter 2: Passive Microrheology Assay

Microrheology refers to a set of measurement techniques in which a microscopic probe object is used to characterize the local viscous, elastic, or viscoelastic properties of a material such as a polymer, biological gel, or colloid solution (40-43). Microrheology techniques rely on the time-dependent mean-square displacement (MSD) of the probe object, generally a microsphere, to provide information about the mechanical properties of the material surrounding the probe. Particle displacement is induced exclusively by Brownian thermal motion (passive microrheology) or by application of an external force (active microrheology) with an optical trap or another similar technique (42). Passive microrheology experiments are fast and can be applied to a wide range of materials from low viscosity fluids to stiff gels (42, 44). This chapter will describe the development and utility of a passive microrheology technique to assess plasma clot stiffness and interrogate the contributions of platelets and fibrin fibers to clot mechanical stiffness and viscoelasticity.

2.1 Background

2.1.1 Brownian Thermal Motion and Mean Squared Displacement

Brownian thermal motion is the random displacement of a microscopic particle suspended in a fluid as a result of collisions with the atoms of the fluid (45). When a microscopic particle is in a purely viscous solution and is able to diffuse freely through the fluid the particle will undergo a random walk (Figure 2.1A) in which the particle moves randomly and unpredictably throughout the fluid (46). However, in a polymer fluid or a fibrous gel the microscopic particle's motion can be limited by the fluid's structure (40,

42, 47). In this case the particle does not undergo a random walk but rather can be “caged” by the material if the particle is larger than the pore size of the material (Figure 2.1B). If the probe particle is smaller than the pore size, it will diffuse through the material but will be inhibited by the material’s structure.

Particle motion in both a caged and freely diffusing scenario can be used to calculate the mean squared displacement (MSD) of the particle. The assay described here will rely on single particle tracking.

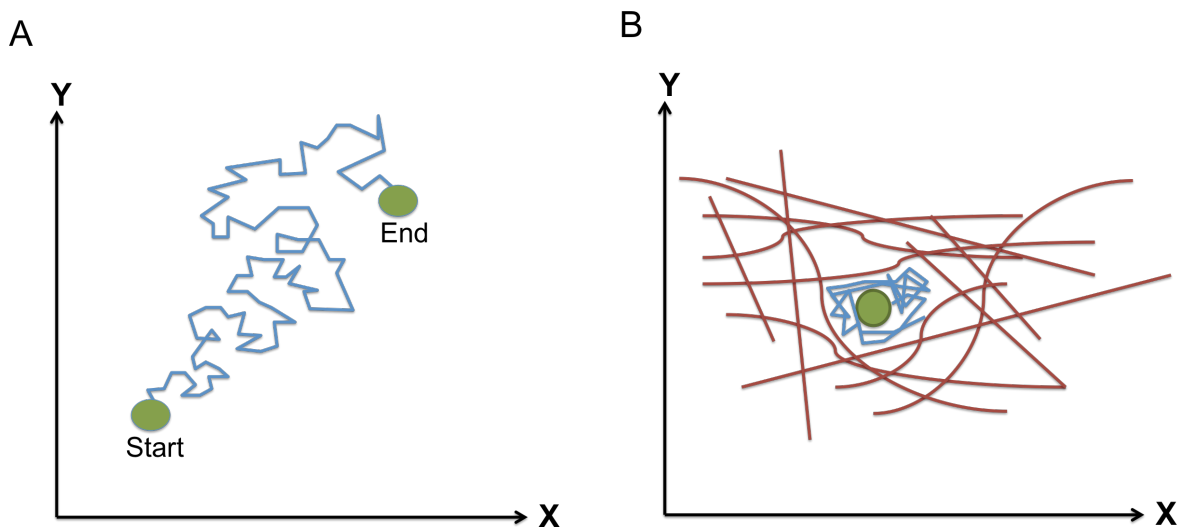


Figure 2.1: Particle motion induced by thermal energy. (A) uninhibited random particle diffusion through a fluid (Brownian thermal motion). (B) limited motion of a particle caged by fibers.

The mean squared displacement of a probe object is related to the viscosity of a fluid through the Stokes-Einstein Equation (40, 41, 43):

$$\langle \Delta r^2(t) \rangle = 2dDt \quad (1)$$

$$D = \frac{k_B T}{6\pi\eta R} \quad (2)$$

where $\langle \Delta r^2(t) \rangle$ is MSD as a function of time, d is the dimensionality, D is the diffusion coefficient, and t is time over which displacement was measured, also known as lag time (40, 45). Equation 1 relates the MSD to the diffusion coefficient, D , which can be used to solve for the viscosity of the fluid using Equation 2, where k_B is the Boltzmann constant, T is temperature, η is viscosity, and R is the radius of the probe particle (48).

The MSD of a particle can provide sufficient information to distinguish between purely viscous fluids and viscoelastic materials. Purely viscous materials will exhibit an approximately linear MSD that does not reach a maximum value over the observed time (41, 47). The Stokes-Einstein equation can be used to calculate the diffusion coefficient of a purely viscous fluid, where the slope of the MSD curve is equal to $4*D$. Viscoelastic materials will exhibit a nonlinear MSD that is characteristic of anomalous diffusion, where particle motion is limited by the structure of the viscoelastic material. The effective diffusion coefficient in anomalous diffusion is related to the MSD through a power law relationship as follows:

$$\langle \Delta r^2 \rangle = \Gamma * t^{(\alpha-1)} \quad (3)$$

$$D_{eff} = \frac{\Gamma * t^{(\alpha-1)}}{2*n} \quad (4)$$

where Γ is the transport factor, n is the dimensionality, and α is a parameter which determines whether the anomalous diffusion is characterized as subdiffusive ($\alpha < 1$) or superdiffusive ($\alpha > 1$) (49).

Probe objects embedded in viscoelastic gels are ‘caged’ by the network if the particle is larger than the pore size of the material, as shown in Figure 2.1B, and undergo anomalous diffusion. Caging of the particle limits the MSD since particle motion is

restricted by the network that it is embedded in, thus correlating MSD and the stiffness of the material.

2.1.2 Dynamic Modulus

Equations 1 through 4 are useful for calculating the diffusion coefficient. However, analysis of the MSD can be extended when considering viscoelastic materials, to calculate the viscoelastic modulus, G :

$$G(\omega) = G'(\omega) + iG''(\omega) \quad (5)$$

where $G'(\omega)$ is the elastic component and $G''(\omega)$ is the viscous component. The viscoelastic modulus is measured in the frequency space, ω , and is related to the mean-square displacement through the Generalized Stokes Einstein Relationship (GSER) (48):

$$\tilde{G}(s) = \frac{k_B T}{\pi a s \langle \tilde{r}^2(s) \rangle} \quad (6)$$

where s is the Laplace frequency and $\langle \tilde{r}^2(s) \rangle$ is the Laplace transform of the mean-squared displacement. The viscoelastic modulus $G(\omega)$ is obtained from $\tilde{G}(s)$ by replacing the Laplace frequency, s , in the GSER with $i\omega$. Analysis of the viscoelastic modulus is not presented in this thesis, but can be completed and presented in future work.

2.2 Methods

2.2.1 Experimental Setup

Whole blood was collected from healthy volunteers in 2.7 mL 3.2% sodium citrate Vacutainer® tubes (BD, Franklin Lakes, NJ, USA) by venipuncture. Whole blood was centrifuged at 100 x G for 20 min to separate platelet rich plasma (PRP) from red blood cells. PRP was collected from the Vacutainer tubes and aliquotted into 0.5 mL samples.

PRP samples for passive microrheology experiments are prepared as follows. 300 nm fluorescent (TRITC) polystyrene microspheres (Polybead, Polysciences, Warrington, PA, USA) are added to each 0.5 mL sample as the probe particles. Fibrinogen is fluorescently labeled by adding fibrinogen from human plasma conjugated to Oregon Green 488 (Sigma, St. Louis, MO, USA). After addition of microspheres and fluorescent fibrinogen, samples are treated with the fab fragment antibody abciximab (ReoPro) (Eli Lilly Company, Indianapolis, IN) at a concentration of 18 $\mu\text{g/mL}$ (a high concentration of ReoPro) or the peptide Gly-Pro-Arg-Pro (GPRP) (Sigma, St. Louis, MO, USA) at a concentration of either 2mM or 4mM or left untreated (referred to as PRP in results). ReoPro binds competitively to integrin $\alpha_{\text{IIb}}\beta_3$ on the platelet surface, preventing fibrinogen from binding to the platelet (20, 21). The GPRP peptide binds to fibrin and prevents fibrin polymerization (39). To initiate clotting, samples are recalcified with CaCl_2 (Sigma, St. Louis, MO, USA) to bring the sample to a concentration of approximately 9.5 mM CaCl_2 . Sample preparation is further detailed in Figure 2.2A.

After calcium is added back to the plasma, 15 μL of the sample is immediately transferred to a large glass coverslip (24 x 60 mm, No. 1 coverglass). The sample is covered with a small glass coverslip (18 x 18 mm, No. 1 coverglass) as shown in Figure

2.2B. Contact with the charged glass surface induces clotting in the sample through the intrinsic pathway (Figure. 1.1). The sample was transferred to a microscope (Diaphot 300, Nikon, Melville, NY, USA) and imaged using a 60X oil lens. Particle motion was recorded for 30 seconds every minute for 15 minutes after clotting was initiated. Microsphere motion was recorded using a video camera (Canon Vixia HF S21, Canon, Melville, NY, USA). Fluorescence images of fibrin structure were taken approximately 20 minutes after clotting was initiated using an Olympus IX51 microscope with a 40x air objective (Olympus America, Center Valley, PA, USA) and a Retiga-4000RV digital CCD camera (QImaging, Burnaby, BC, Canada) controlled via Q-Capture Pro 7 software (QImaging, Burnaby, BC, Canada).

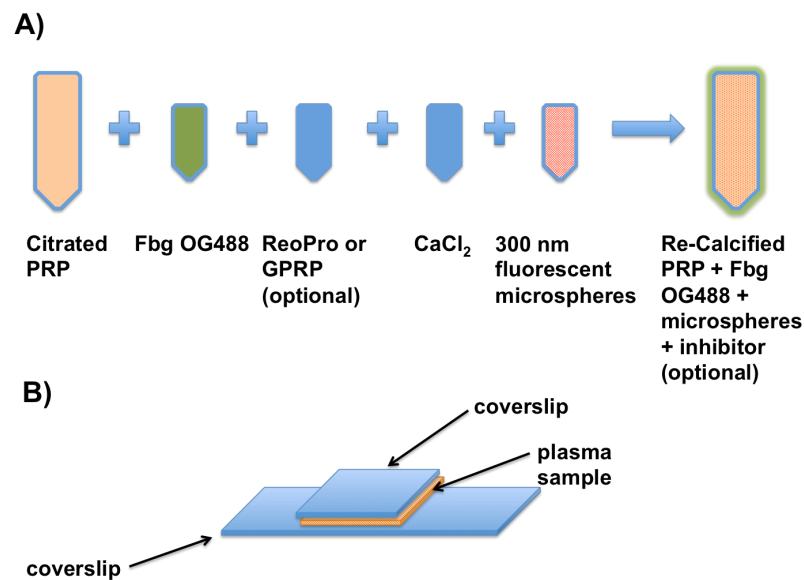


Figure 2.2: Sample preparation and experimental setup for passive microrheology experiments. (A) Sample handling steps. (B) Coverslip setup used for imaging.

2.2.2 Data Analysis

Single particle tracking and video microscopy are utilized to obtain the X and Y position of microspheres in treated and untreated plasma samples for 15 minutes after

coagulation was initiated. A custom automated tracking algorithm was used to track microsphere position in ImageJ (NIH, Bethesda, MD, USA). Video was recorded at 30 frames per second for 5 seconds, resulting in a total of 150 video frames with X and Y position data for each frame. A video was taken every minute for 15 minutes after coagulation was initiated, and a total of five microspheres were tracked in each video. MSD is calculated using $n = 5$ microspheres and a lag time ranging from 1 video frame (1/30 seconds) to 150 video frames (5 seconds) using a custom Matlab (Natick, MA, USA) function.

MSD curves are used to calculate the effective diffusivity (diffusion coefficient) of microspheres in plasma. The plasma samples are not characteristic of a purely viscous fluid and thus a power law relationship is used to fit a curve through the MSD using the “FIT” function in Matlab. R^2 and goodness of fit are calculated using Matlab and an effective diffusivity is calculated using equations 3 and 4.

Fluorescence images are quantified using a custom algorithm developed by David Vorp, PhD and his group at the University of Pittsburgh (50). The algorithm utilizes binary fluorescence images to create a skeleton of the original image and calculates mean fiber diameter, tortuosity, two dimensional porosity, and fiber concentration.

2.3 Results

2.3.1 Mean Squared Displacement and Effective Diffusivity

The mean squared displacement of polystyrene microspheres is calculated in human plasma during coagulation using $n = 5$ microspheres. Plasma was either left untreated (PRP) or treated with GPRP or ReoPro. Clotting was initiated through the

intrinsic coagulation pathway and microsphere motion due to Brownian thermal motion was recorded for 15 minutes.

MSD curves for all samples at 5 minutes after coagulation were characteristic of anomalous diffusion, opposed to free diffusion, indicating that the sample is not a purely viscous fluid (Figure 2.3- Figure 2.6). The nonlinear nature of the MSD curve suggests that viscoelasticity has developed to some extent in all four samples. MSD can be modeled using a power law relationship.

MSD curves for all samples look remarkably different at 10 minutes after coagulation, compared to the MSD at 5 minutes, except for the sample treated with 4mM GPRP. The MSD in PRP, 2 mM GPRP, and 18 $\mu\text{g}/\text{mL}$ ReoPro is nearly a horizontal line and MSD magnitude is on the order of $10^{-4} \mu\text{m}^2/\text{sec}$ for PRP and ReoPro, compared to $\sim 10 \mu\text{m}^2/\text{sec}$ at 5 minutes after coagulation (Figure 2.3- Figure 2.6). The MSD magnitude at 10 minutes is also reduced compared to 5 minutes, although to a lesser extent than in PRP and ReoPro treated samples. The horizontal line and low magnitude of MSD combined suggest that the microspheres are no longer moving, likely due to caging effects. The only sample that did exhibit a horizontal line at 10 minutes after coagulation was the sample treated with 4 mM GPRP. The MSD curve for 4mM GPRP treated plasma retained a power law shape; although, the magnitude of MSD was reduced approximately two fold, compared to MSD at 5 minutes.

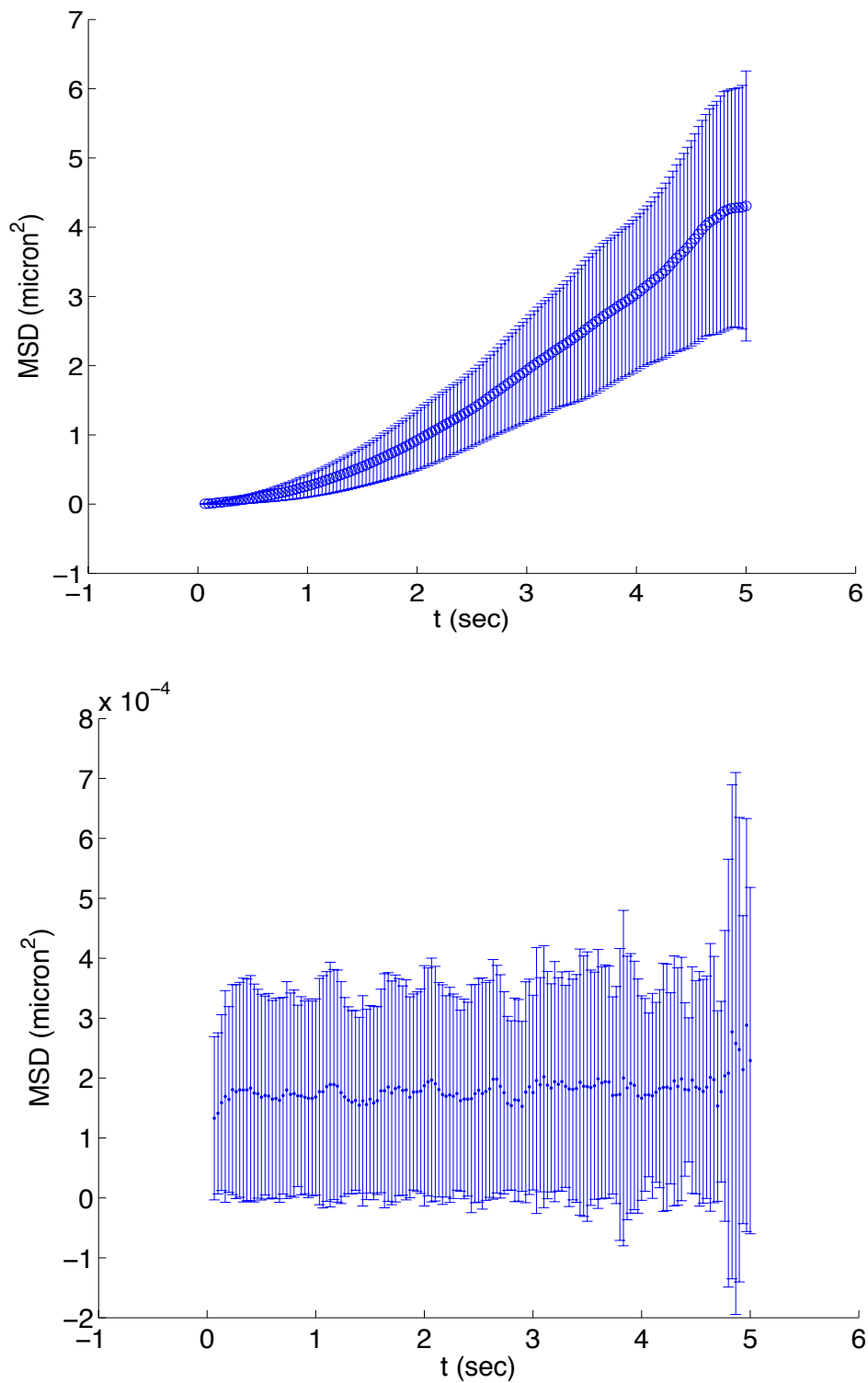


Figure 2.3: Mean squared displacement of 300 nm microspheres in untreated human plasma (PRP). Top: MSD 5 minutes after coagulation was initiated. Bottom: 10 minutes after coagulation was initiated.

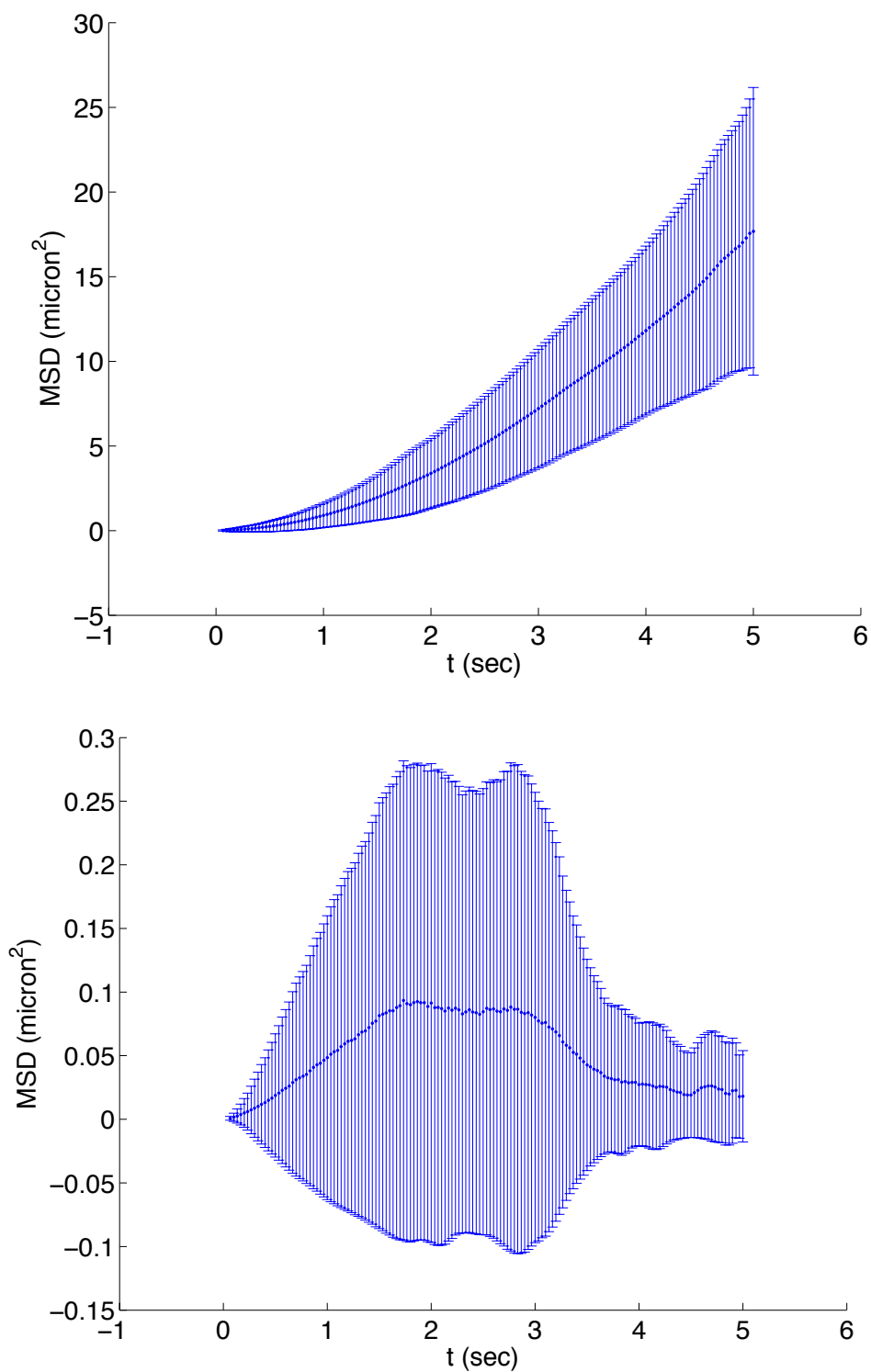


Figure 2.4: Mean squared displacement of 300 nm microspheres in human plasma treated with 2 mM GPRP peptide inhibitor. Top: MSD 5 minutes after coagulation was initiated. Bottom: 10 minutes after coagulation was initiated.

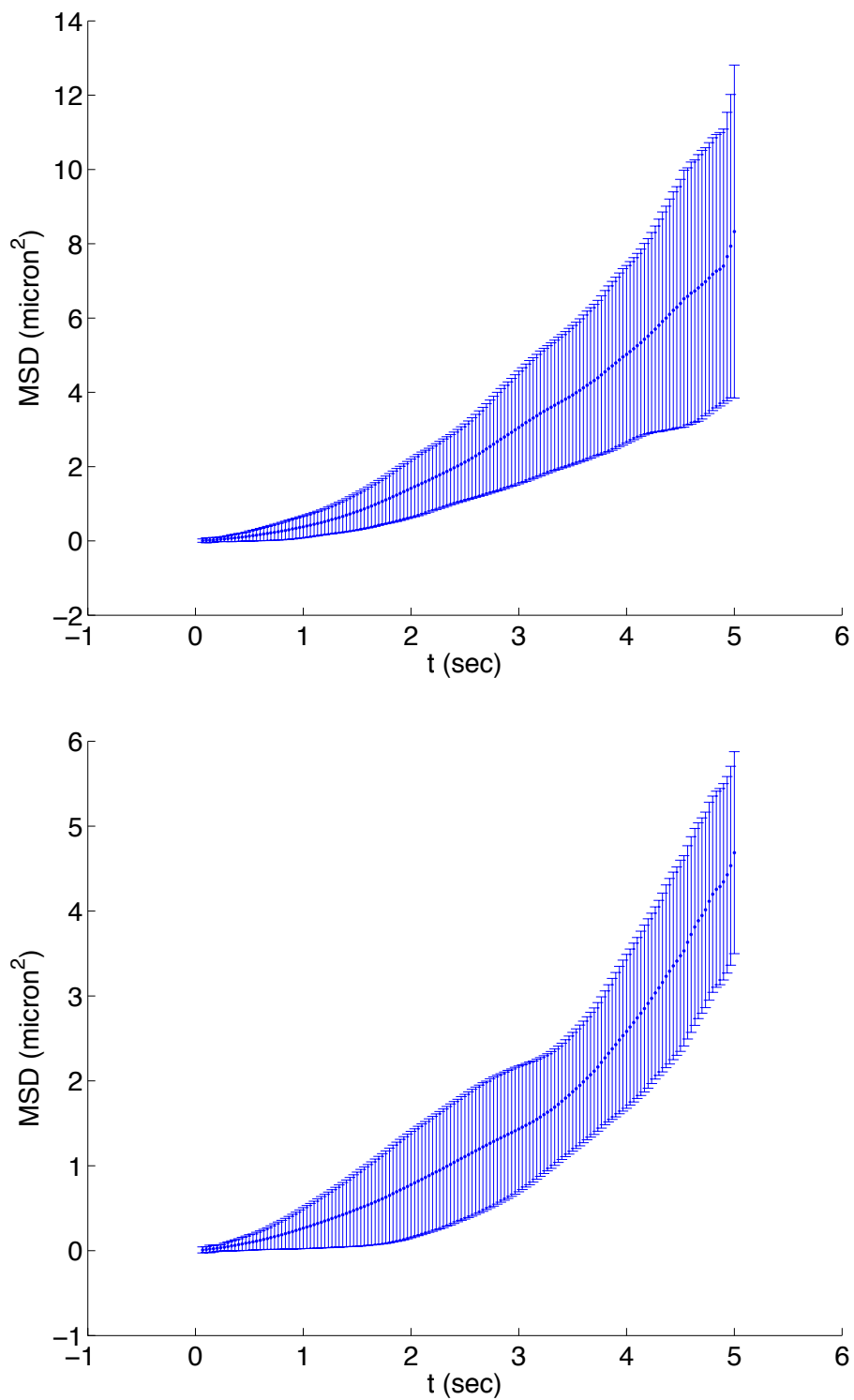


Figure 2.5: Mean squared displacement of 300 nm microspheres in human plasma treated with 4 mM GPRP peptide inhibitor. Top: MSD 5 minutes after coagulation was initiated. Bottom: 10 minutes after coagulation was initiated.

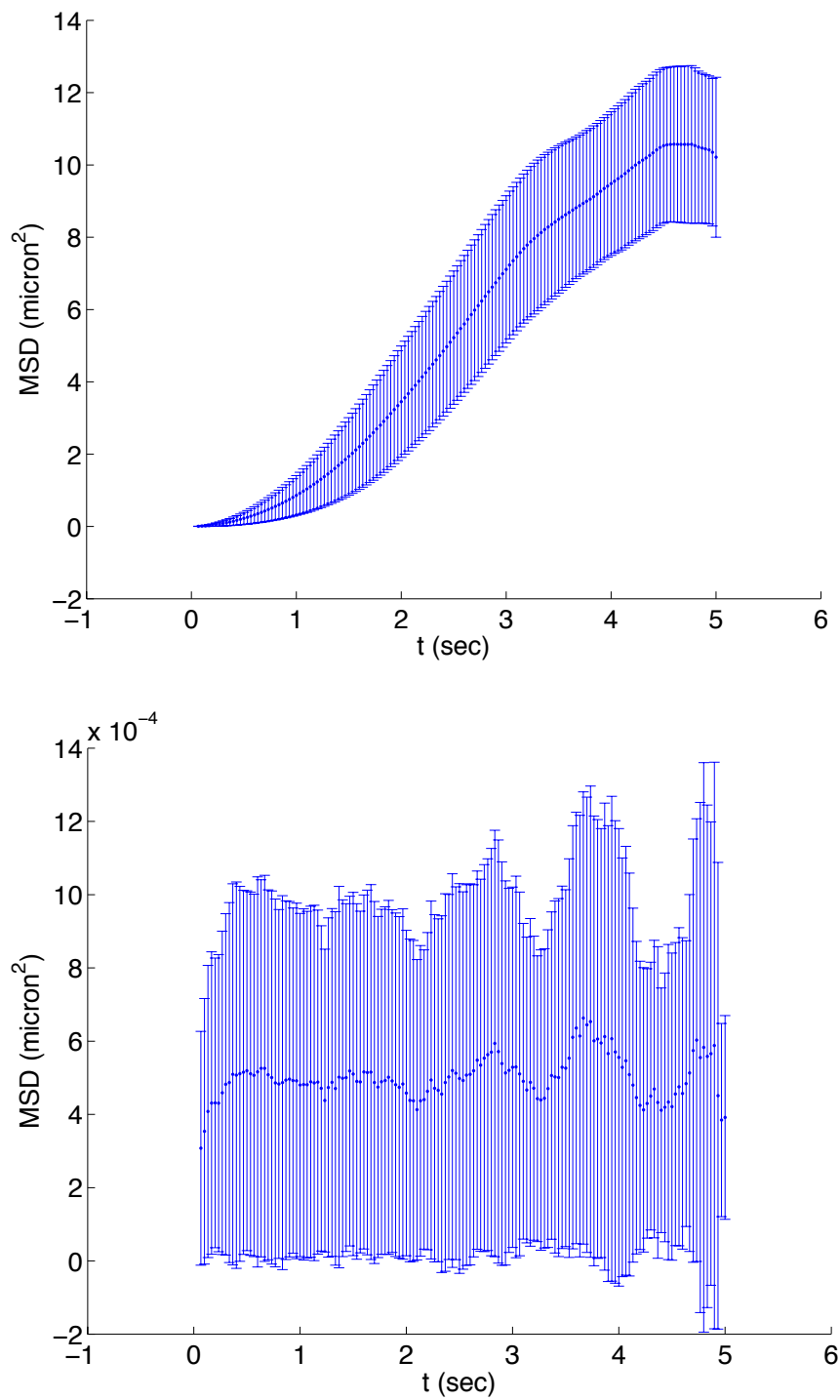


Figure 2.6: Mean squared displacement of 300 nm microspheres in human plasma treated with 18 $\mu\text{g}/\text{mL}$ ReoPro fab fragment antibody. Top: MSD 5 minutes after coagulation was initiated. Bottom: 10 minutes after coagulation was initiated.

After mean squared displacement was calculated, curve fitting was used to calculate the effective diffusivity. A power law fit was calculated in the form of Equation 3 and Equation 4 was used to calculate effective diffusivity. An example power law fit is shown in Figure 2.7. The power law curve shown for PRP at 5 minutes after coagulation demonstrates a good fit to the MSD data, where $R^2 > 0.999$ and $\chi^2 \sim 1$.

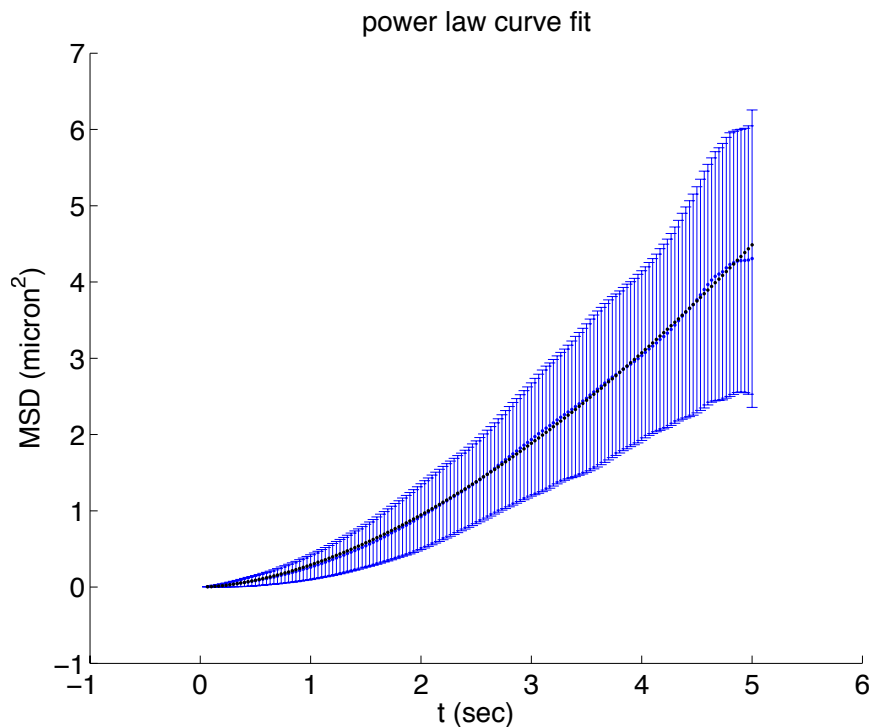


Figure 2.7: Power law curve fit to experimental mean squared displacement for a PRP sample 5 minutes after coagulation was initiated. Error bars represent standard deviation; power law fit is represented as a black line ($R^2 > 0.999$, and χ^2 goodness of fit ~ 1).

Effective diffusivity was calculated for each sample every minute after coagulation (Figure 2.8 and Figure 2.9). Effective diffusivity of the microspheres decreases sharply within the first several minutes of coagulation and continues to decrease to approximately zero in all samples, except for 4 mM GPRP treated plasma. The effective

diffusivity of 4 mM GPRP treated plasma remains constant at approximately $0.26 \mu\text{m}^2/\text{sec}$ from 8 minutes after coagulation through the duration of the experiment (15 minutes).

Individual effective diffusivity curves are presented for all four samples in Figure 2.9.

Effective diffusivity curves versus time follow the same trend; a large initial decrease in diffusivity followed by a gradual decrease in diffusivity until microspheres become caged or the diffusivity reaches a steady value. This suggests an early development of clot mechanical properties and may be useful in identifying a gel point for the clot.

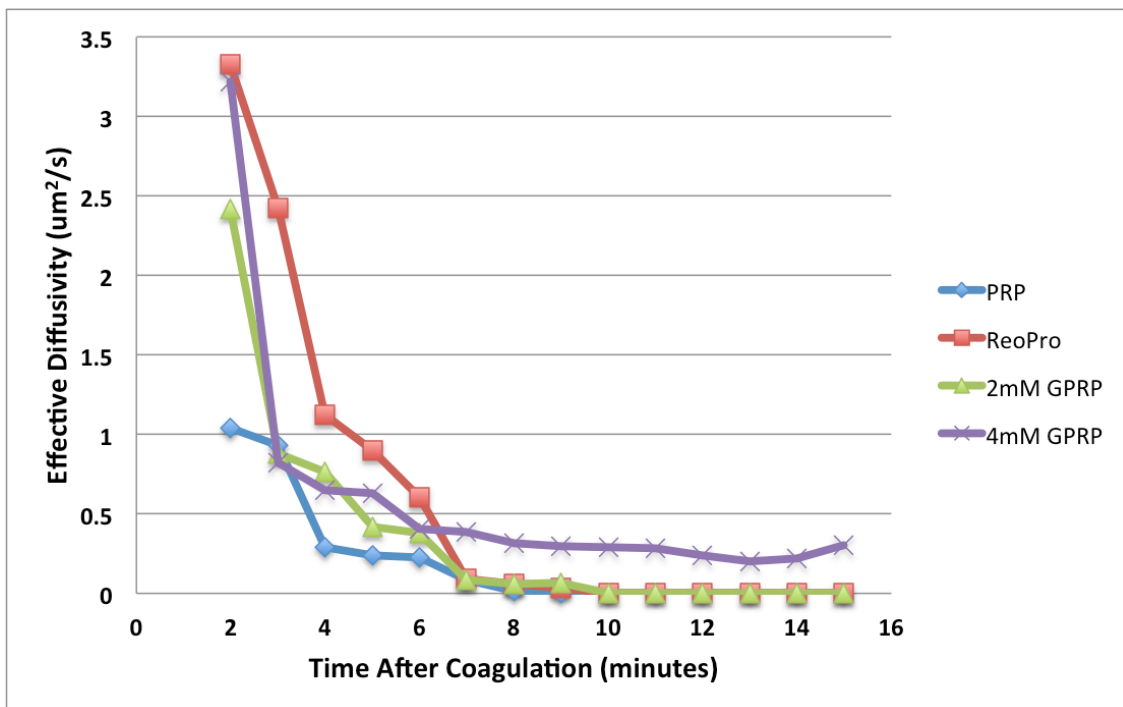


Figure 2.8: Effective diffusivity of 300 nm microspheres in human plasma during coagulation.

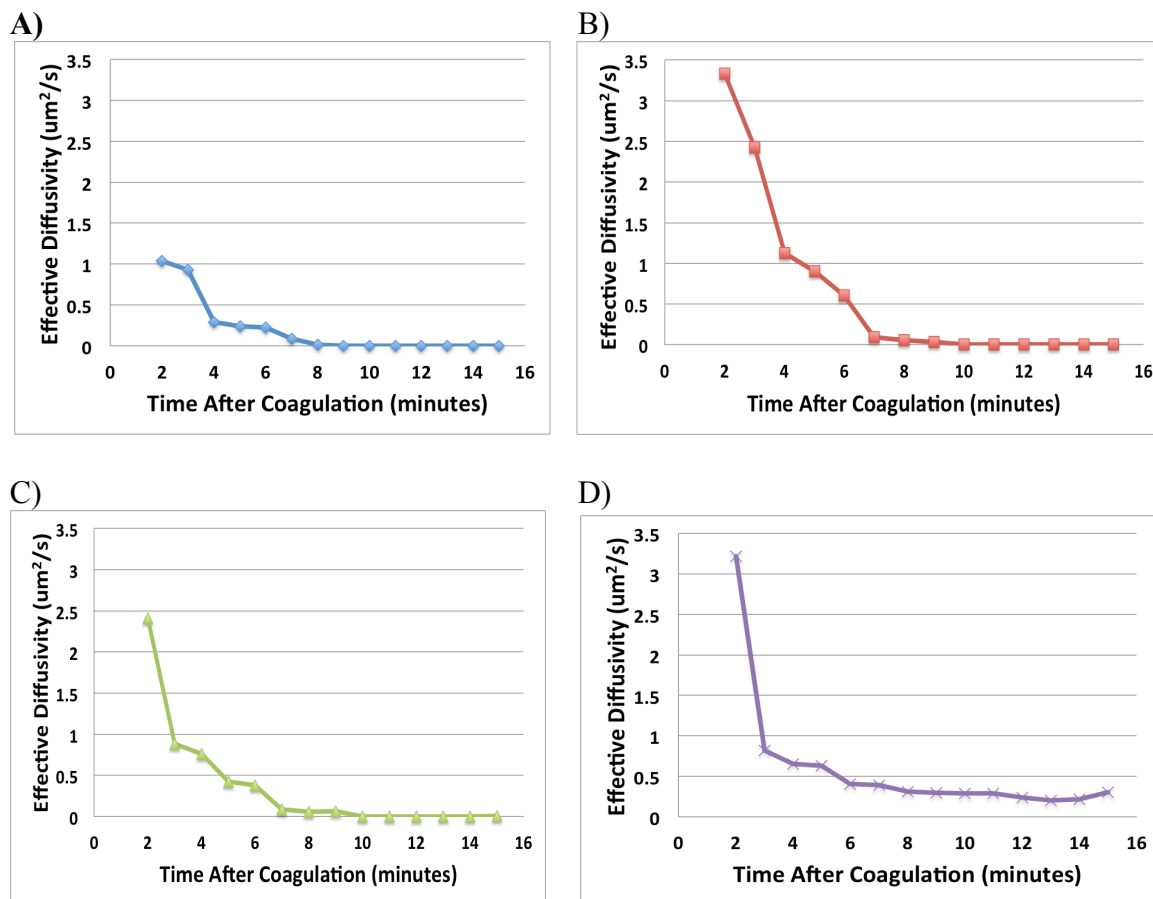


Figure 2.9: Effective diffusivity of a 300 nm fluorescent microsphere in human plasma. Microspheres were dispersed in A) PRP, B) PRP treated with 18 ug/mL ReoPro, C) PRP treated with 2 mM GPRP, and D) PRP treated with 4 mM GPRP.

2.3.2 Fluorescence Images

Fluorescence imaging of blood plasma samples with fluorescently labeled fibrinogen (fibrinogen conjugated to Oregon Green 488) is used to correlate mechanical information from microtheology experiments with the structural features of a clot. Fluorescence images are presented in Figure 2.10- Figure 2.12.

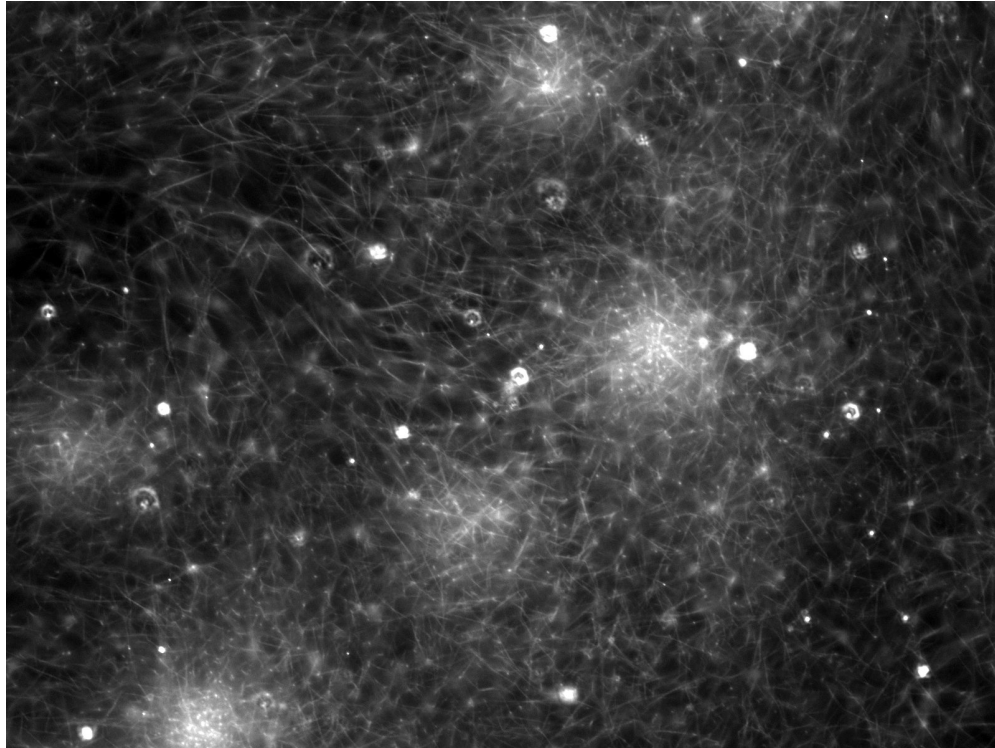


Figure 2.10: Fluorescence image of a blood plasma clot with Oregon Green 488 labeled fibrinogen. 40X magnification.

Fluorescence images of untreated PRP show a typical clot structure with a high fibrin fiber density, network crosslinking, and platelet aggregations. Treatment with the fibrin polymerization inhibitor GPRP peptide results in structural differences in the clot network. When PRP is treated with 4 mM GPRP the fibrin fiber density and crosslinking decreases and fewer platelet aggregates are seen (Figure 2.12). From visual observation of the images, it appears that network porosity is greatly increased when 4 mM GPRP is applied, compared to untreated PRP. Treatment with 2 mM GPRP shows an intermediate effect between untreated PRP and 4 mM GPRP (Figure 2.11).

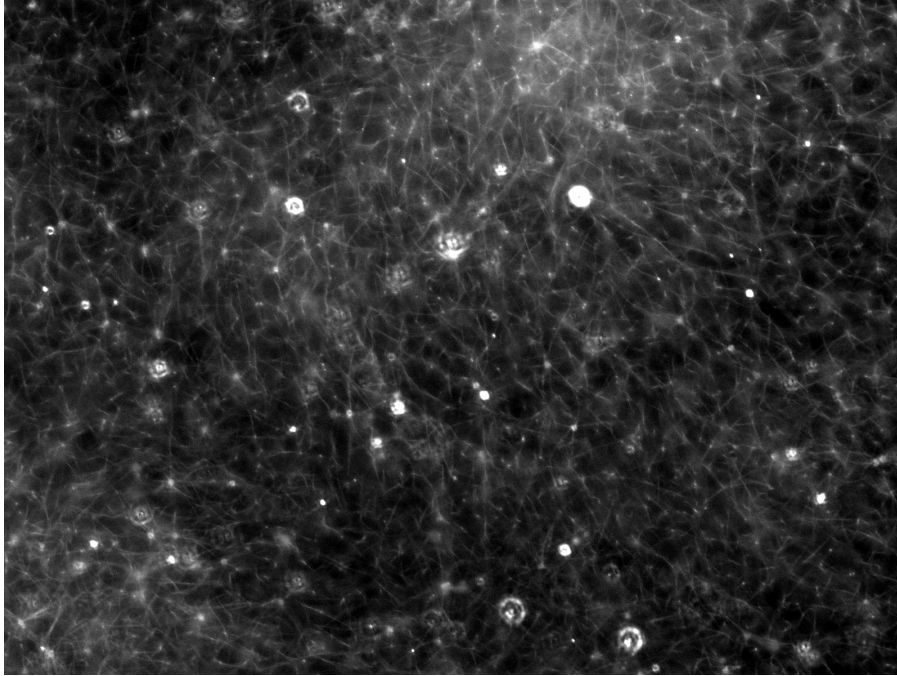


Figure 2.11: Fluorescence image of a 2 mM GPRP treated blood plasma clot with Oregon Green 488 labeled fibrinogen. 40X magnification.

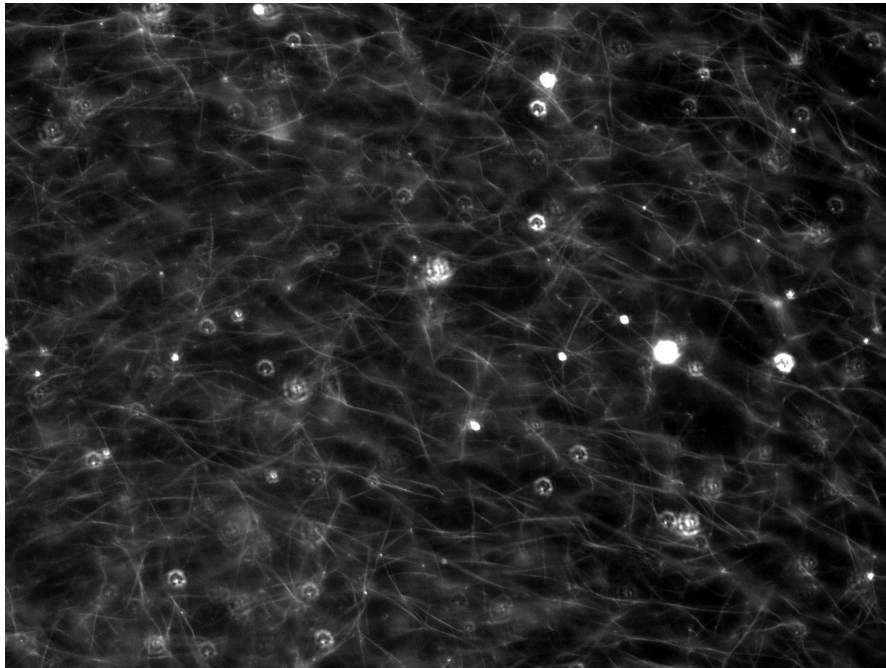
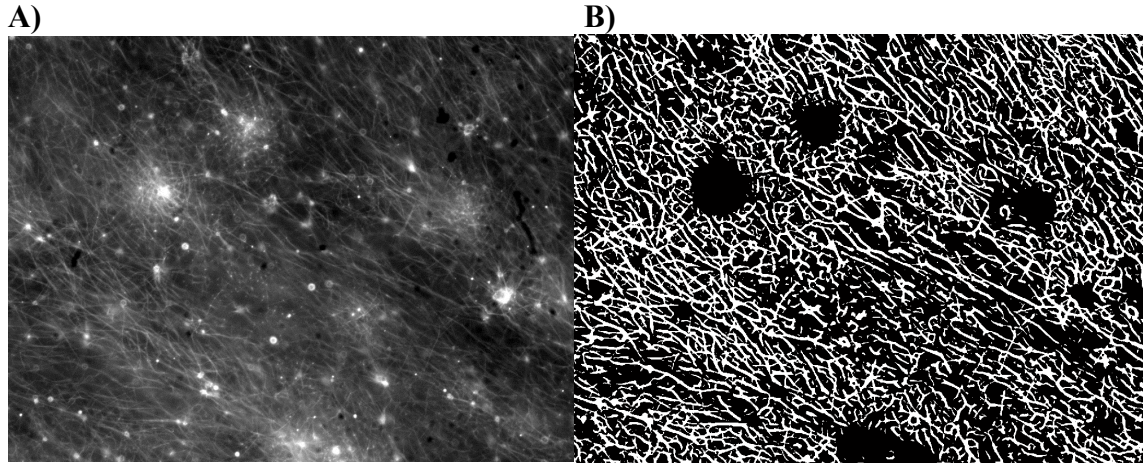


Figure 2.12: Fluorescence image of a 4 mM GPRP treated blood plasma clot with Oregon Green 488 labeled fibrinogen. 40X magnification.

Quantitative analysis of fluorescence images can be used to correlate mechanical properties with structural features of blood plasma clot networks such as porosity, tortuosity, and fibrin fiber diameter. A custom image analysis algorithm developed by Koch et al (50) was implemented to examine the structural features of fibrin networks under two conditions, untreated PRP and ReoPro treated. The results of the analysis are presented in Fig. 2.13 and Fig 2.14.

The custom analysis algorithm converts a fluorescence image to a binary skeletonized image that represents the fibrin fiber network. The skeletonized image is then analyzed for various structural features. The results of preliminary analysis demonstrate the utility of the custom algorithm and can be used in the future to assess samples that have been treated with a drug or inhibited in another way.

The custom algorithm was able to detect differences in porosity between the untreated PRP and ReoPro treated images. Two-dimensional porosity was measured to be 69.38 in untreated PRP and 84.91 in the ReoPro treated sample. The lower porosity in untreated PRP is indicative of a smaller pore size and correlates with increased fiber concentration. The results of the image analysis are presented in Table 2.1.



C)

```

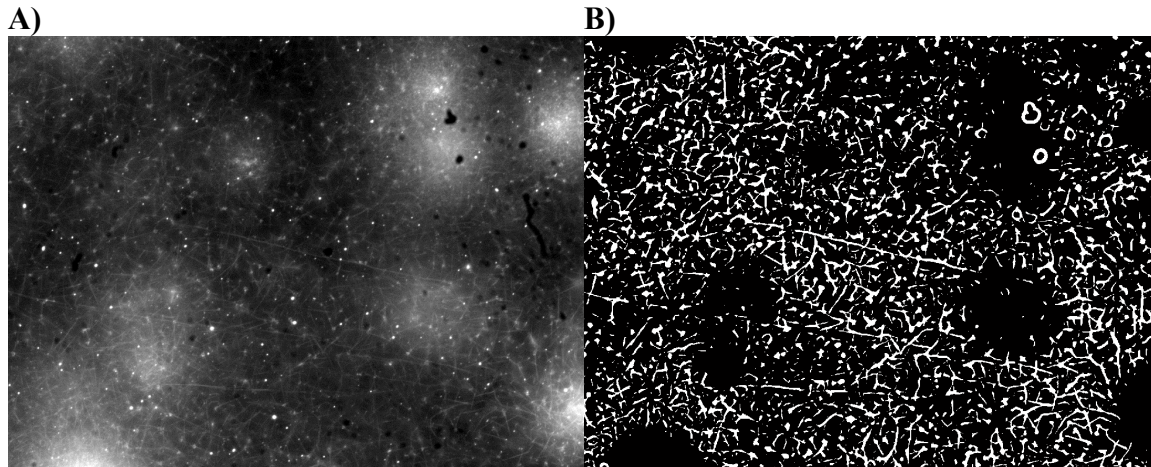
The fiber diameter used is: 6.000000
Creating fiber skeleton...

Calculating branch points and pruning skeleton...
Calculating outputs...
Generating figures...
Finding vertically running components...
Calculating tortuosity of large segments
Calculating fiber orientation...

Intersection Fiber Density (Intersects/Fiber Area) = 0.0026
Fiber Concentration = 30.6201
2D Porosity = 69.3799
Tortuosity = 1.1113 +/- 0.3463
Average Segment Length = 25.0860 +/- 21.4646
Mean Fiber Orientation = 77.4418 +/- 47.7641
Radial Counts Percentage = 6.6998
Horizontal Counts Percentage = 9.4293
Mean Fiber Diameter = 5.3305 +/- 2.4065

```

Figure 2.13: Structural analysis of an untreated PRP clot using custom image analysis algorithms developed by Koch et al. A) Fluorescence image of an untreated PRP clot at 40X magnification where fibrin fibers are labeled with Orgeon Green 488. B) Skeletonized fluorescence image of the PRP clot shown in panel A. C) Results of the custom image analysis algorithm which computes, porosity, tortuosity, and mean fiber diameter, in pixels.



C)

```

The fiber diameter used is: 7.000000
Creating fiber skeleton...

Calculating branch points and pruning skeleton...
Calculating outputs...
Generating figures...
Finding vertically running components...
Calculating tortuosity of large segments
Calculating fiber orientation...

Intersection Fiber Density (Intersects/Fiber Area) = 0.0007
Fiber Concentration = 15.0838
2D Porosity = 84.9162
Tortuosity = 1.2986 +/- 1.3682
Average Segment Length = 28.8068 +/- 23.8823
Mean Fiber Orientation = 99.9482 +/- 50.9270
Radial Counts Percentage = 9.7784
Horizontal Counts Percentage = 13.0704
Mean Fiber Diameter = 4.9124 +/- 2.3096

```

Figure 2.14: Structural analysis of ReoPro treated PRP (18 $\mu\text{g}/\text{mL}$) clot using custom image analysis algorithms developed by Koch et al. A) Fluorescence image of a PRP clot at 40X magnification where fibrin fibers are labeled with Orgeon Green 488. B) Skeletonized fluorescence image of the PRP clot shown in panel A. C) Results of the custom image analysis algorithm which computes, porosity, tortuosity, and mean fiber diameter, in pixels.

	PRP	ReoPro
Fiber Concentration (%)	30.62	15.08
2D Porosity (%)	69.38	84.91
Tortuosity	1.11	1.29
Mean Fiber Diameter (pixels)	5.33 +/- 2.4065	4.91 +/- 2.31

Table 2.1: Structural analysis PRP and ReoPro treated fluorescence images. Analysis was done using an algorithm developed and described by Koch et al.

2.4 Discussion

The findings of the passive microrheology experiments are significant because they demonstrate the ability of the assay to detect the development of mechanical properties in both untreated samples and samples that have been perturbed. Confirmation that the passive microrheology measurement is sensitive enough to detect differences in clot viscoelasticity is promising to identify the origins of clot stiffness.

This work demonstrates differences in the effective diffusivity of microspheres in four different samples. MSD curves showed noticeable changes in shape as coagulation progressed. In PRP, 2 mM GPRP treated plasma, and 18 $\mu\text{g}/\text{mL}$ ReoPro treated plasma the slope of the MSD curve decreased with time until the MSD was near zero and could be approximated by a horizontal line. The decrease in the slope of the line is indicative of a viscoelastic transformation, the development of clot stiffness, and caging or trapping of the microspheres in the fibrin fiber network.

A change in slope with time was not seen as dramatically, however, in 4 mM GPRP treated plasma, indicating that the microspheres were not trapped in the fiber network. The lack of caging in 4 mM GPRP treated samples is likely due to a larger pore

or cage size in the network, allowing the microsphere to diffuse through the network. This observation is supported by the apparent decrease in cross-linking and large pore size seen in fluorescence images of plasma treated with 4 mM GPRP (Figure 2.12). This finding is not surprising as GPRP is a competitive inhibitor of fibrin fiber polymerization. It is also interesting to note that ReoPro treatment did not have a detectable effect on the MSD and viscoelastic transformation of the sample. The lack of effect is interesting since ReoPro concentrations above 12 $\mu\text{g/mL}$ have been shown to inhibit clot stiffness (23). Quantitative analysis of fluorescence images showed a two fold decrease in fiber concentration after treatment with ReoPro, yet the effective diffusivity is similar between PRP and ReoPro treated plasma. It is possible that ReoPro treatment does not directly affect cage size, even though there are fewer fibers present in the field of view. It is also possible that the passive microrheology assay is not sensitive enough to detect rheological differences in ReoPro treated plasma. The measurement is sensitive enough, however, to detect rheological differences in samples in which fibrin polymerization has been perturbed.

Mean squared displacement curves were used to calculate the effective diffusivity of microspheres in each sample. Although changes in the shape of MSD curve are generalized as changes in slope, the MSD is not a linear curve. The MSD in all samples is best characterized by a power law function. Curve fitting was used to obtain the Γ and α parameters needed to compute the effective diffusivity, using Equation 4. Goodness of fit was calculated for the power law fit in each sample at each time point to ensure the model was representative of the observed data. From 2 minutes after coagulation until approximately 8 minutes after coagulation, the power law goodness of fit was very good

($R^2 > 0.98$). After MSD curves become approximately horizontal at approximately 8 minutes, the power law fit begins to break down. The loss of a good fit is not surprising, as the microspheres are no longer undergoing diffusion, anomalous or otherwise. A linear fit was also tested, although the goodness of fit was not as good as the power law fit.

Effective diffusivity data in plasma demonstrates the utility of the passive microrheology measurement in quantifying the rheological properties of blood plasma clots, as well as detecting changes in the rheological properties of plasma during coagulation. The effective diffusivity information as a function of coagulation time can be used to detect differences in the time to clot as well as any endpoint differences in the rheological properties.

After validation of passive microrheology as a sensitive rheological measurement the assay is coupled with fluorescence imaging and image analysis techniques to establish structure-function relationships. The MSD of an individual microsphere can be calculated and used to characterize the clot structure immediately surrounding the particle. Image analysis in the region surrounding the particle can then be used to pair specific structural information with the mechanical information. This technique can be used to probe very specific regions of the clot or it can be generalized over a larger clot region by averaging the MSD of many microspheres in the clot. After MSD has been calculated the dynamic modulus can be calculated to further characterize the viscoelasticity of the plasma clot. This analysis will be useful to determine the contribution of platelets, fibrin fiber diameter, tortuosity, and fibrin fiber crosslinking to the mechanical properties of fibrin networks.

Chapter 3: Acoustic Radiation Force Assay

3.1 Background

Active microrheology is a broad set of measurement techniques that relies on the application of external forces to a sample in order to characterize the mechanical properties of the material. Many active rheological methods exist such as rotational rheometers, optical tweezers or laser trap, and atomic force microscopy, among others. The assay described here is an active rheological method that relies on the application of ultrasound to probe a blood plasma clot.

A novel ultrasound acoustic radiation force based method is used to displace acoustically reflective polystyrene microspheres dispersed in blood plasma samples to actively perturb the fibrin fiber network. The custom sample chamber allows sample perturbation by ultrasound ARF and optical tracking of microspheres dispersed in the sample to occur simultaneously.

Acoustic radiation force arises from an ultrasound wave incident on an object in the wave's path (32, 33). The particle can absorb and reflect the energy of the ultrasound wave and thus feels a body force. As a result of the body force, ARF can be used to induce displacement of particles embedded in a material, such as a viscoelastic gel, and Stokes' Law can be used to determine the magnitude of the applied acoustic radiation force when the particle is spherical (51).

$$F = 6 \pi \mu R v \quad (7)$$

Equation 7 is Stoke's Law where F is applied force, μ is the viscosity, R is the particle radius, and v is the particle velocity. ARF displacement of microparticles is a noncontact method of inducing strain in a material. Also, in addition to being a well-characterized force, the magnitude of applied ARF is tunable by altering the parameters of the ultrasound setup such as the pulse repetition frequency or the center frequency of the ultrasound transducer.

3.2 Methods

3.2.1 Experimental Setup

Whole blood is collected from healthy volunteers in 2.7 mL 3.2% sodium citrate Vacutainer® tubes (BD, Franklin Lakes, NJ, USA) by venipuncture. Whole blood is centrifuged at 100 x G for 20 min to obtain PRP. Additional centrifugation at 2000 x G for 40 min is used to obtain platelet poor plasma (PPP). PRP is collected and aliquotted into a 2 mL sample volume. Plasma from multiple tubes, from the same donor, is pooled to obtain 2 mL total sample volume. 15 μm polystyrene microspheres (Polybead, Polysciences, Warrington, PA, USA) are added to each sample. PRP samples are contained in the custom sample chamber (Figure 3.1) during testing. To initiate clotting, samples are recalcified with CaCl_2 (Sigma, St. Louis, MO, USA) to bring the PRP to a concentration of ~ 9.5 mM CaCl_2 . Kaolin (JT Baker, VWR, Radnor, PA, USA) is added to a final concentration of 5 $\mu\text{g}/\text{mL}$ to initiate clotting through the intrinsic pathway (Figure 1.1). Clotting and the ARF pulsing sequence are initiated within 15 s of kaolin addition. Particle motion within the sample is recorded for 30-second intervals every 3 minutes throughout the initial 30 minutes after clotting was initiated.

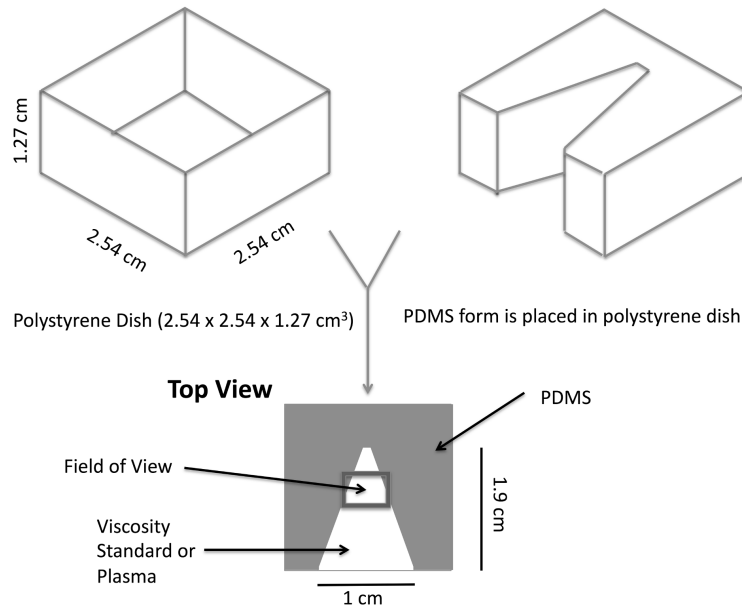


Figure 3.1: Custom sample holder consists of polystyrene dish with a PDMS insert. The shape of the PDMS insert reduces volume requirements for the blood sample, while the PDMS material properties allow it to act as an ultrasonic absorber reducing ultrasound wave reflection in the chamber.

The experimental setup consists of a platform, which aligns the ultrasound transducer relative to the microscope objective such that the transducer focus and microscope objective focus are aligned (Figure 3.2). The sample was held in place over the objective and acoustically coupled to the transducer with ultrasound gel (Aquasonic, Parker Laboratories, Fairfield, NJ, USA). A 2.54 cm square polystyrene box (8.2 mL) (Ted Pella, Redding CA, USA) was used to hold the plasma sample. An acoustically absorbent V-shaped polydimethylsiloxane form (Figure 3.1) was inserted into the box to minimize acoustic reflections and reduce the required sample volume to 2 mL. A 10 MHz single-element focused transducer (model IBMF103, NDT Systems, Huntington Beach, CA, USA) was used for this work. The 10 MHz transducer has a diameter of 9.5 mm and a

focal length of 19 mm. The transducer and sample holder are held in place by a custom stage mounted on an air table. The sample holder was mounted above a microscope (Diaphot 300, Nikon, Melville, NY, USA) with a 10 X microscope air objective, which permitted focusing into the sample at varying depths. For optimal foci alignment of the ultrasound beam with the objective plane of focus, the optical focal plane was fixed at 1300 μm above the sample holder surface for all stiffness measurements. The motion of microspheres dispersed within the sample was recorded at 30 frames per second by a video camera (Canon Vixia HF S21, Canon, Melville, NY, USA) mounted to the microscope camera port. As microspheres experiencing ARF move more slowly than material shear waves due to their size relative to fundamental material components (e. g. molecules, fibers), standard frame rate (30 fps) video microscopy can be used to assess microsphere trajectories with a high degree of precision.

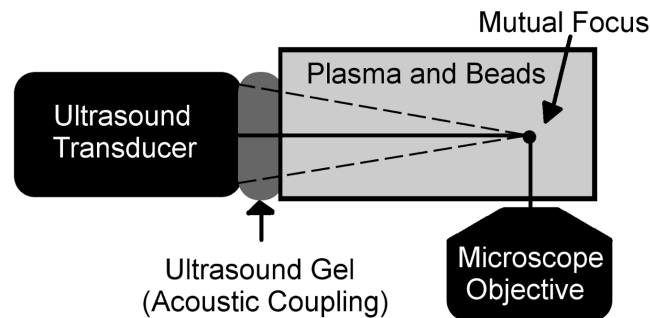


Figure 3.2: The ARF based measurement setup used a 10 MHz ultrasound transducer to apply ARF to blood plasma in which microspheres were suspended. A microscope with 10 X objective and video camera had a mutual focus with the ultrasound transducer so application of ARF to the sample could be observed in the microscope field of view.

The magnitude of applied ARF must be known to calculate clot stiffness from microsphere displacement. The magnitude of applied ARF was estimated by tracking microspheres and measuring terminal velocity in known viscosity fluids. Stokes' law was applied to determine the force on an object moving through a fluid of known viscosity. Three fluids with known viscosities were used to calibrate ARF on the microspheres. Two NIST traceable viscosity standards (S3 and S6) (Cole Parmer, Court Vernon Hills, IL, USA) and anticoagulated blood plasma were used.

To estimate force, 15 μm diameter latex polystyrene microspheres were suspended in the fluid samples (Polybead, Polysciences, Warrington, PA, USA). The S3 and S6 fluids have precisely known viscosities of 4.063 cP and 8.743 cP, respectively, at 25° C. At room temperature blood plasma has a viscosity of 1.6 ± 0.1 cP (52).

The 10 MHz transducer used to generate ARF was triggered in all experiments by a custom amplifier circuit connected to a Macbook laptop computer (Apple, Cupertino, CA) running a Matlab/C++ program that controlled the ultrasound transducer firing pattern. A 0.8 μs pulse length (8 wave cycles) was applied. We define the rate of pulse generation used to create an impulse sequence by a pulse repetition frequency (PRF). Pulses were generated at a PRF of 7.5 kHz over a pulse interval of 0.5 s. Pulse intervals were separated by 6 s of rest. In place of the custom amplifier circuit, a waveform generator and power amplifier can be substituted to increase dynamic range in selected experiments.

To investigate the effect of changing the PRF on microsphere displacement the PRF was varied in the viscosity standards. PRFs of 15, 7.5, 3.75, and 1.875 kHz were used

at a time interval of 0.5 s. The result was a total of 7500, 3750, 1875, and 937 pulses fired per burst for each respective condition.

3.2.2 Data Analysis

Two methods of single particle tracking implemented in the image processing software ImageJ (NIH, Bethesda, MD, USA) were used to quantify microsphere displacement due to incident ARF: a manual particle tracking protocol and an automated tracking algorithm (53). Manual tracking was used when microsphere velocities were greater than 400 $\mu\text{m/s}$ and the automated algorithm was used in all other cases. At high velocities manual tracking was more accurate due to edge detection limitations in the automated tracking algorithm. The automated tracking algorithm utilized a cross-correlation technique to measure sub-pixel and sub-micron displacements (54). Manual tracking was performed using the point tool in ImageJ with the “auto-measure” and “auto-next slice” features turned on.

Clot stiffness in PPP was determined by the equation:

$$S = \frac{F_{plasma}}{D_m}, \quad (8)$$

where S is the clot stiffness, F_{plasma} is the ARF applied to microspheres in plasma, and D_m is the average of microsphere maximum displacements after application of 0.5 s of an ARF pulse. As a form of Hooke’s law, the inverse relationship between applied force and resultant displacement defines stiffness (S) (Equation 8) (55).

3.3 Results

3.3.1 Microsphere Displacement

The magnitude of ARF applied to microspheres in clotting blood plasma is estimated by measuring displacements in anticoagulated PRP and two viscosity standards, using microsphere motion velocity to calculate the applied force using Stokes' law (Equation 7). Microsphere motion in anticoagulated PRP was compared to that in viscous standards. Terminal microsphere velocities during ARF application were measured (Figure 3.3a) and Stokes' law for drag force was used to calculate the force applied to the microspheres (Figure 3b) (51).

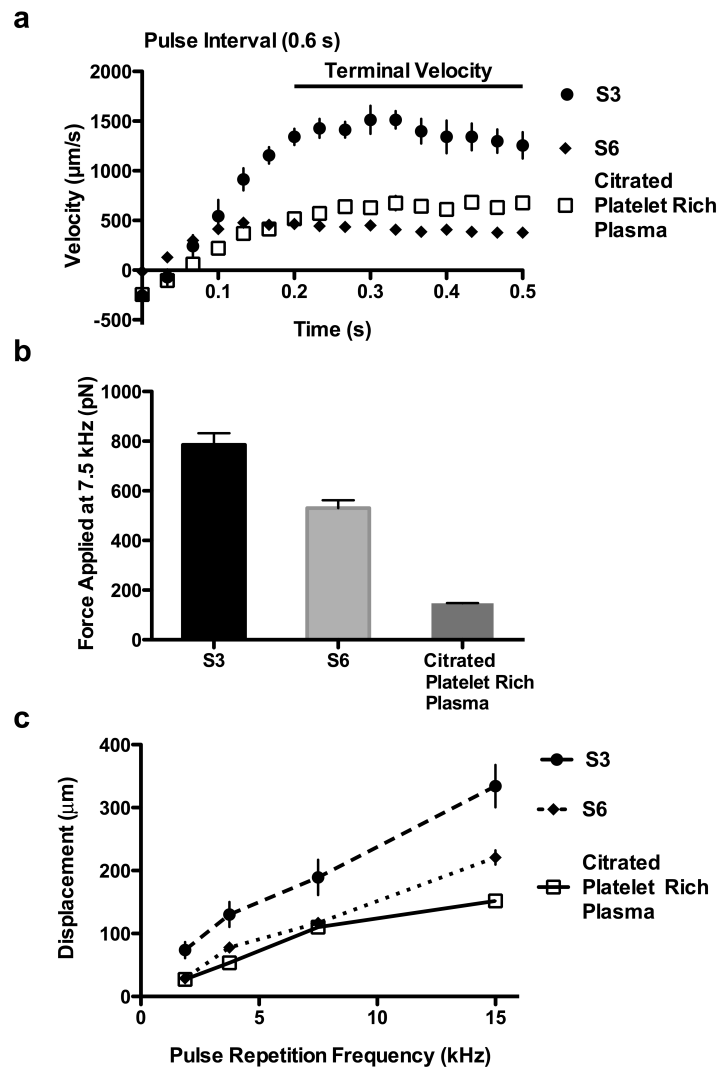


Figure 3.3: (a) Microsphere terminal velocities were measured under applied ARF at 7.5 kHz PRF in the viscosity standards S6 (8.743 cP) and S3 (4.063 cP), and in citrated plasma. Standard error is shown with n=10 microspheres. (b) Applied ARF magnitude at 7.5 kHz was determined using Stokes' law and terminal microsphere velocities. It is thought that distinct acoustic attenuations between the fluids account for much of the difference in the applied force in the fluids. At 7.5 kHz the force applied in citrated blood plasma was estimated to be 147 pN. Standard error is shown with n=10 microsphere. (c) Microsphere displacement after 0.3 s of pulsing due to applied ARF increased linearly with increasing PRF in the three fluids. Standard error is shown with n=9 microspheres.

The microsphere terminal velocities in the viscosity standards S6 (8.743 cP at room temperature) and S3 (4.063 cP at room temperature) and citrated PRP (1.6 cP at room temperature) (52) were $429.4 \pm 57.2 \mu\text{m/s}$, $1367.4 \pm 256.4 \mu\text{m/s}$, and $646.5 \pm 120.4 \mu\text{m/s}$ respectively. From Stokes' law (Equation 7) it was determined that the ARF magnitude applied at 7.5 kHz pulse repetition frequency on the microspheres in S6, S3, and citrated PRP was $530.7 \pm 70.7 \text{ pN}$, $785.4 \pm 147.3 \text{ pN}$, and $147.0 \pm 27.2 \text{ pN}$ respectively (Figure 3.3). The differences in the applied force on the microspheres may reflect differences in the degree of ultrasound attenuation between the three fluids

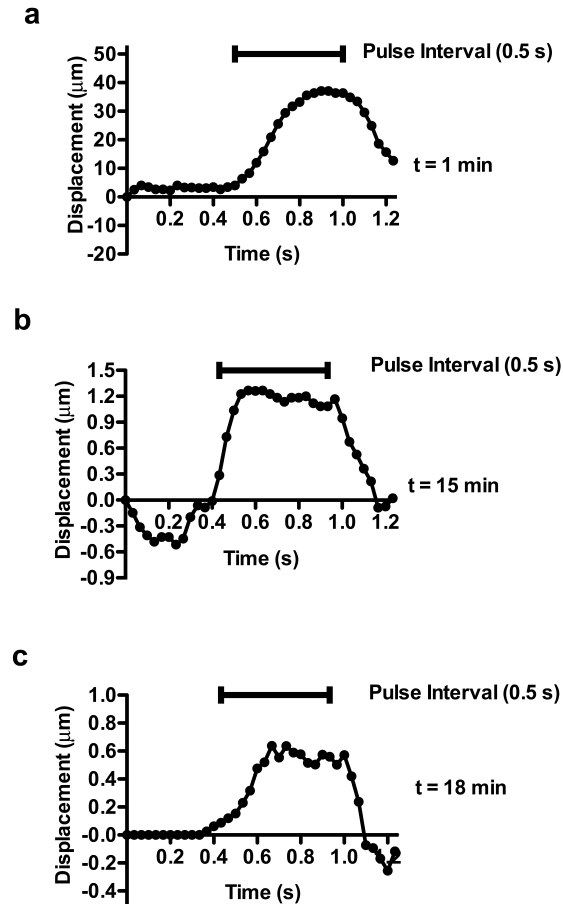


Figure 3.4: Characteristic microsphere displacement due to applied ARF at 7.5 kHz in clotting platelet poor plasma. (a) At $t = 1$ min the microsphere is displaced 40 μm during a 0.5 s pulse interval and recoiled after the pulse stopped. (b) At $t = 15$ min the microsphere is displaced 0.9 μm during the pulse interval and recoiled after the pulse stopped. (c) At $t = 18$ min the microsphere is displaced 0.5 μm during the pulse interval and recoiled after the pulse stopped.

3.3.2 Clot Stiffness

The stiffness of ReoPro treated samples and PPP samples were compared to PRP clot stiffness to assess platelet contributions to clot stiffness (Figure 3.5 And Figure 3.6, respectively). ReoPro treatment and platelet removal both resulted in decreased clot stiffness relative to PRP and delayed development of clot stiffness. ReoPro treatment decreased clot stiffness by approximately 1.8 fold (Figure 3.5) and platelet removal

decreased clot stiffness by approximately 7.9 fold (Figure 3.6). These results demonstrate the ability of the ARF assay to detect and quantify mechanical differences in different samples.

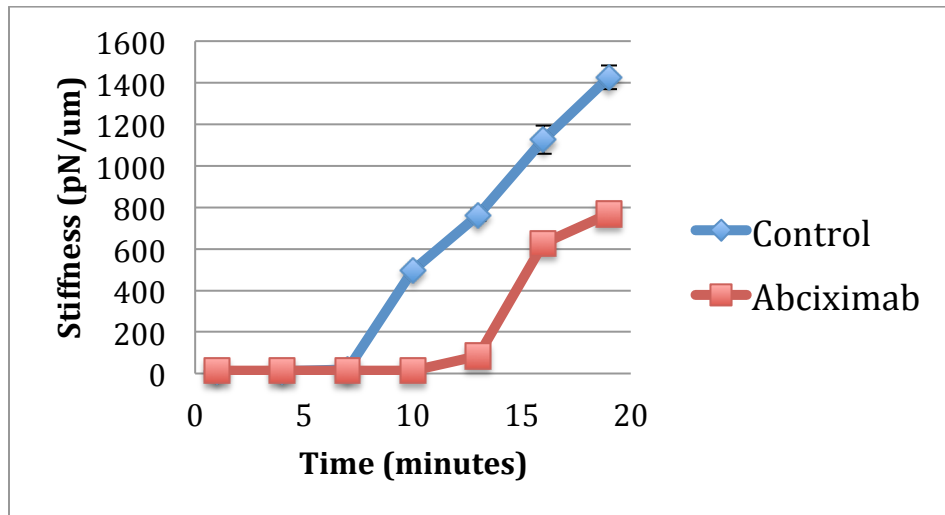


Figure: 3.5 Clot stiffness in untreated PRP (control) and PRP treated with 18 $\mu\text{g/mL}$ ReoPro (Abciximab) assessed by application of ARF at 7.5 kHz. Clot stiffness $S(t) = F_{\text{plasma}}/Dm_{\text{avg}}$, was determined for both samples using microsphere displacements. The average displacement of microspheres in the sample ($n = 5$) was used to compute stiffness. Error bars represent standard deviation.

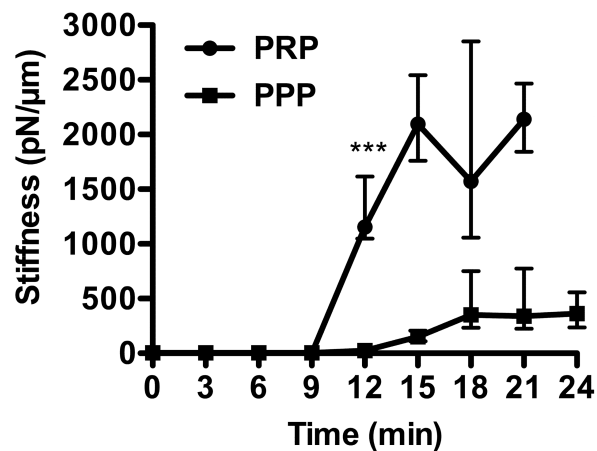


Figure 3.6: Characteristic mechanical properties of clotting platelet rich (PRP) and platelet poor plasma (PPP) as assessed by application of ARF at 7.5 kHz. Clot stiffness (S), $S(t) = F_{\text{plasma}}/Dm_{\text{avg}}$, of clotting PRP and PPP was determined. Microsphere

displacements ($n = 5$) were averaged to compute stiffness, which is displayed with 60% quartiles (***, $p < 0.0005$ between PPP and PRP from $t > 12$ min).

3.4 Discussion

The optical ARF assay described in this work is capable of detecting differences in clot stiffness under normal and perturbed conditions. Two platelet-specific perturbations were used to validate the assay. The motion of microspheres under applied ARF is initially dominated by blood plasma viscosity and later, as clotting progresses, is marked by increased elasticity. A clear effect on clot stiffness was seen when a platelet inhibitor was added to PRP and when platelets were removed by centrifugation. A delay in the development of clot stiffness and a decrease in clot stiffness relative to untreated PRP control are observed with both perturbations. So, this assay shows utility for studies on both early stages of clot development and studies on fully developed clots.

The detection of viscoelastic material properties by ARF-induced bead motion has several experimental limitations. A microscope-based bead tracking approach has an inherent stiffness detection limit defined by video resolution and the optical signal to noise ratio; i.e, once the gel becomes very stiff relative to the force on the bead, motion stops. Further increases in gel stiffness are undetectable after that point is reached. However, improved signal detection can be achieved by increasing transducer power to increase e displacement or by raising microscope magnification to increase spatial resolution. Increases in plasma clot turbidity, which becomes a significant optical limitation after 45 minutes, can also reduce bead displacement measurement accuracy. Fluorescent beads can be used to allow optical ARF analysis at advanced stages of PRP clot development (~1 h).

An additional benefit of the ARF assay is that the force application is variable and easily controlled by altering the ultrasound parameters. By varying the PRF, the force per bead could be varied from 10 - 294 pN. These forces are on the order of those required for rupture of a fibrin fiber bond (200 pN) or to stretch a monomer in a fibrin fiber to 100% strain (140 pN). Since rupture of fibrin fibers in a network requires greater force than that needed to rupture a single fibrin bond, it is assumed that the forces applied by ARF in this study are largely non-destructive to the fibrin network, allowing evaluation of its viscoelasticity. This assertion is also supported by the elastic recoil seen when microsphere displacement is plotted (Figure 3.4).

The passive acoustic radiation force approach is a non-destructive assay that has sufficient sensitivity to detect differences in clot stiffness after platelet perturbation. The dynamic and tunable nature of the force development makes this a useful tool to analyze platelet contributions to clot stiffness.

References

1. Weisel, J (2008) Enigmas of Blood Clot Elasticity. *Science*. 320:456–457.
2. Ryan E, Mockros L, Weisel J, Lorand L (1999) Structural origins of fibrin clot rheology. *Biophysical Journal*. 77:2813–2826.
3. Tran R et al (2013) Biomechanics of haemostasis and thrombosis in health and disease: from the macro- to molecular scale. *Journal of Cellular and Molecular Medicine*. 17:579–596.
4. Weisel J (2010) Biomechanics in hemostasis and thrombosis. *Journal of Thrombosis and Hemostasis*. 8:1027–1029.
5. Chitlur M et al (2008) Thromboelastography in children with coagulation factor deficiencies. *British Journal of Hematology*. 142:250–256.
6. Essell J et al (1993) Comparison of thromboelastography to bleeding time and standard coagulation tests in patients after cardiopulmonary bypass. *Journal of Cardiothoracic and Vascular Anesthesiology*. 7:410–415.
7. Elliott A et al (2015) Thromboelastography in patients with acute ischemic stroke. *International Journal of Stroke*. 10:194–201.
8. Collet J et al (2006) Altered fibrin architecture is associated with hypofibrinolysis and premature coronary atherothrombosis. *Arterioscler Thromb Vasc Biol*. 26:2567–2573.
9. Lam W et al (2010) Mechanics and contraction dynamics of single platelets and implications for clot stiffening. *Nature Materials*. 10:61–66.
10. Kashluk J et al (2009) Rapid thrombelastography (r-TEG) identifies hypercoagulability and predicts thromboembolic events in surgical patients. *Surgery*. 146:764–774.
11. Weisel JW, Litvinov RI (2013) Mechanisms of fibrin polymerization and clinical implications. *Blood*. 121:1712-1719.
12. Chernysh IN, Nagaswami C, Purohit PK, Weisel JW (2012) Fibrin Clots Are Equilibrium Polymers That Can Be Remodeled Without Proteolytic Digestion. *Scientific Reports* 2.
13. Phillips DR, Charo IF, Parise LV, Fitzgerald LA (1988) The platelet membrane glycoprotein IIb-IIIa complex. *Blood*. 136:239.

14. Lewis JC et al. (1990) Fibrinogen and glycoprotein IIb/IIIa localization during platelet adhesion. Localization to the granulomere and at sites of platelet interaction. *The American Journal of Pathology* 136:239.
15. Bennett J (2006) Platelet-Fibrinogen Interactions. *Annals of the New York Academy of Sciences* 936:340–354.
16. Parekh PJ, Merrell J, Clary M, Brush JE, Johnson DA (2014) New Anticoagulants and Antiplatelet Agents: A Primer for the Clinical Gastroenterologist. *The American Journal of Gastroenterology* 109:9–19.
17. Hashemzadeh M, Furukawa M, Goldsberry S, Movahed MR (2008) Chemical structures and mode of action of intravenous glycoprotein IIb/IIIa receptor blockers: A review. *Experimental & Clinical Cardiology* 13:192.
18. Epstein FH, Lefkovits J, Plow EF, Topol EJ (1995) Platelet Glycoprotein IIb/IIIa Receptors in Cardiovascular Medicine. *N Engl J Med* 332:1553–1559.
19. Podolnikova NP et al. (2014) The Interaction of Integrin α IIb β 3 with Fibrin Occurs through Multiple Binding Sites in the α IIb β -Propeller Domain. *J Biol Chem* 289:2371–2383.
20. Tam SH, Sassoli PM, Jordan RE, Nakada MT (1998) Abciximab (ReoPro, Chimeric 7E3 Fab) Demonstrates Equivalent Affinity and Functional Blockade of Glycoprotein IIb/IIIa and α v β 3 Integrins. *Circulation* 98:1085–1091.
21. Topol EJ, Byzova TV, Plow EF (1999) Platelet GPIIb-IIIa blockers. *The Lancet* 353:227–231.
22. Root-Bernstein RS, Westall FC (1984) Fibrinopeptide A binds Gly-Pro-Arg-Pro. *PNAS* 81:4339–4342.
23. Viola F et al. (2010) A novel ultrasound-based method to evaluate hemostatic function of whole blood. *Clinica Chimica Acta*. 411:106–113.
24. Jen CJ, McIntire L (1982) The structural properties and contractile force of a clot. *Cell Motility*. 2:445–455.
25. Carr ME (2003) Development of platelet contractile force as a research and clinical measure of platelet function. *Cell Biochem Biophys*. 38:55–78.
26. Evans PA, Hawkins K, Williams PR (2006) Rheometry for blood coagulation studies. *Rheology Reviews*. 255–291.
27. Shah JV, Janmey PA (1997) Strain hardening of fibrin gels and plasma clots. *Rheola Acta*. 36:262–268.

28. Burghardt WR, Goldstick TK, Leneschmidt J, Kempka K (1995) Nonlinear viscoelasticity and the thrombelastograph: 1. Studies on bovine plasma clots. *Biorheology*. 32:621–630.
29. Fine I, Kaminsky A, Kuznik B, Shenkman L (2011) A non-invasive method for the assessment of hemostasis in vivo by using dynamic light scattering. *Laser Phys*. 22:469–475.
30. Tripathi et al. (2014) Assessing blood coagulation status with laser speckle rheology. *Biomed Opt Express*. 5:817–831.
31. Collet JP et al. (2005) The elasticity of an individual fibrin fiber in a clot. *PNAS*. 102:9133–9137.
32. Torr GR (1984) The acoustic radiation force. *American Journal of Physics*. 52:402–408.
33. Nightingale K (2002) Acoustic radiation force impulse imaging: in vivo demonstration of clinical feasibility. *Ultrasound in Medicine and Biology*. 28:227–235.
34. Nightingale K, McAleavey S, Trahey G (2003) Shear-wave generation using acoustic radiation force: in vivo and ex vivo results. *Ultrasound in Medicine and Biology*. 29:1715–1723.
35. Palmeri ML et al. (2008) Quantifying Hepatic Shear Modulus In Vivo Using Acoustic Radiation Force. *Ultrasound in Medicine and Biology*. 34:546–558.
36. Negron L et al. (2002) Development and characterization of a vitreous mimicking material for radiation force imaging. *IEEE Transactions*. 49:1543–1551.
37. Fatemi et al. (2003) Imaging elastic properties of biological tissues by low-frequency harmonic vibration. *Proc IEEE*. 91:1503–1519.
38. Viola F et al. (2004) Sonorheometry: A noncontact method for the dynamic assessment of thrombosis. *Annals of Biomedical Engineering*. 32:696–705.
39. Mauldin FW et al. (2010) Adaptive force sonorheometry for assessment of whole blood coagulation. *Clinica Chimica Acta*. 411:638–644.
40. Cai L-H, Panyukov S, Rubinstein M (2011) Mobility of Spherical Probe Objects in Polymer Liquids. *Macromolecules* 44:7853–7863.
41. Gardel ML, Valentine MT, Weitz DA (2005) in *Microscale Diagnostic Techniques* (Springer Berlin Heidelberg, Berlin/Heidelberg), pp 1–49.
42. Pietro Cicuta, Donald AM (2007) Microrheology: a review of the method and applications. *Soft Matter* 3:1449–1455.

43. Gisler T, Weitz DA (1998) Tracer microrheology in complex fluids. *Current Opinion in Colloid & Interface Science* 3:586–592.
44. Gittes F, Schnurr B, Olmsted PD, MacKintosh FC, Schmidt CF (1997) Microscopic Viscoelasticity: Shear Moduli of Soft Materials Determined from Thermal Fluctuations. *Phys Rev Lett* 79:3286–3289.
45. Mansel BW, Williams M, Patten PJ, Keen S, Hemar Y (2013) *A Practical Review of Microrheological Techniques*.
46. Wilson LG, Harrison AW, Schofield AB, Arlt J, Poon WCK (2009) Passive and Active Microrheology of Hard-sphere Colloids. *J Phys Chem B* 113:3806–3812.
47. Squires TM, Mason TG (2009) Fluid Mechanics of Microrheology. <http://dxdoi.org/10.1146/annurev-fluid-121108-145608> 42:413–438.
48. Mason TG (2000) Estimating the viscoelastic moduli of complex fluids using the generalized Stokes–Einstein equation. *Rheol Acta* 39:371–378.
49. Wu J, Berland KM (2008) Propagators and Time-Dependent Diffusion Coefficients for Anomalous Diffusion. *Biophysical Journal* 95:2049–2052.
50. Koch RG et al. (2014) A custom image-based analysis tool for quantifying elastin and collagen micro-architecture in the wall of the human aorta from multi-photon microscopy. *Journal of Biomechanics* 47:935–943.
51. Dayton PA et al. (2002) The magnitude of radiation force on ultrasound contrast agents. *Journal of the Acoustic Society of America*. 112:2183–2192.
52. Shinton N (2010) *Desk Reference for Hematology* (CRC Press, Boca Raton). 2nd Ed.
53. Schneider CA et al. (2012) NIH Image to ImageJ: 25 years of image analysis. *Nature Methods*. 9:671–675.
54. Cheezum M, Walker W, Guilford W (2001) Quantitative comparison of algorithms for tracking single fluorescent particles. *Biophysical Journal*. 81:2378–2388.
55. Hooke R (1678) *Lectures de potentia restitutiva, or, Of spring: explaining the power of springing bodies: to which are added some collections* (Printed for J. Martyn).